FEATURE ARTICLE

Design, fabrication and characterization of PCL electrospun scaffolds—a review

A. Cipitria,[ab] A. Skelton,[a] T. R. Dargaville,[a] P. D. Dalton[ac] and D. W. Hutmacher*[ad]

The expanding interest in electrospinning fibers for bioengineering includes a significant use of polyesters, including poly(ε-caprolactone) (PCL). This review summarizes literature on PCL and selected blends, and provides extensive descriptions of the broad range of parameters used in manufacturing such electrospun fibers. Furthermore the chemical, physical and biological approaches for characterizing the electrospun material are described and opinions offered on important information to include in future publications with this electrospun material.

1 Introduction

The origins of the electrospinning process can be traced to the first half of the 20th century through various patents by Cooley,[1] Morton[2] (both 1902), Norton[3] (1936) and by Formhals in the 1930s and 1940s.[4–7] The technique was not commercially adopted due to competition with mechanical drawing processes to form polymeric fibers, and electrospinning remained an obscure method of making fibers until the mid-1990s. At this time, Reneker and colleagues demonstrated its potential for nano-technology research, since the polymeric material produced was both sub-micron in diameter and inexpensive to prepare.[8] Additionally, electrospinning could be used with a variety of diverse polymeric materials and readily accommodated within a research laboratory.

Electrospun fibers are produced by applying a potential difference (high voltage) between a polymeric liquid and a collecting target. A polymeric fluid with sufficient macromolecular entanglements is typically pumped to the tip of a capillary, or spinneret. When electrical charges overcome the surface tension of the fluid, a polymeric fluid jet is ejected from the spinneret. Due to the macromolecular entanglements, the ejected liquid jet does not undergo Rayleigh instabilities (breaking up of the liquid jet into droplets), but is coherently drawn directly towards the collector. Since the surface charge density increases with proximity to the collector, the charges become sufficiently high to cause a second transformation, where the jet is twisted and

drawn. This phenomenon of fiber drawing is often termed "bending instabilities" and stretches the fibers resulting in the formation of nano-scale fiber materials. When a single collector is used, the fibers are non-woven and the collected material is often called "meshes". Further details of the physical phenomena governing the electrospinning process can be found in numerous articles.[9–22]

About 6 years after the usefulness of electrospinning was demonstrated by Reneker, researchers including the Ko and Bowlin laboratories showed that electrospun fibers are relevant for tissue engineering (TE) research.[23,24] In one respect this is due to electrospun fibers attaining diameters similar to fibrous extracellular matrix (ECM) in the body, in particular collagen. In the subsequent decade, electrospun fiber meshes have attracted increasing attention within TE, including as wound dressing and in skin TE, blood vessel TE, neural TE, bone and cartilage TE or controlled drug release, as described in various reviews.[25–28] The rapid rise in the use of electrospun material for TE can be put down to a number of factors. Firstly, as previously stated, the nanofiber mesh architecture can mimic the hierarchical organized fibrous structure found in the ECM. Secondly, the high surface area of the electrospun meshes is favorable for cell attachment and drug loading. Furthermore, the fibrous porosity facilitates nutrient and waste exchange. There are advantages of electrospinning over other nanofiber mesh fabrication methods such as phase separation or self-assembly. They include the simplicity and low cost of constructing a laboratory device, its versatility—a wide range of possible polymer solutions can be employed, changing the composition in the core/shell of the fibers using coaxial electrospinning and control over fibers diameter and alignment—and reproducibility. While we are not yet at the stage of generating complex electrospun TE structures, the potential and huge interest generated after less than 10 years of research in this area indicates that the process is here to stay and be one of the more important TE scaffold fabrication techniques in the first half of the 21st century. While there is definitely

aInstitute of Health and Biomedical Innovation, Queensland University of Technology, 60 Musk Avenue, Kelvin Grove, Brisbane, QLD, 4059, Australia. E-mail: dietmar.hutmacher@qut.edu.au
bJulius Wolff Institute and Center for Musculoskeletal Surgery, Berlin-Brandenburg Center for Regenerative Therapies, Charité-Universitätsmedizin, Berlin, Germany
cMed-X Research Institute, Shanghai Jiao Tong University, Huashan Lu 1954, Shanghai, 200030, China
*dGeorge W. Woodruff School of Mechanical Engineering, Georgia Institute of Technology, Atlanta, USA*

This journal is © The Royal Society of Chemistry 2011

J. Mater. Chem., 2011, **21**, 9419–9453 | 9419
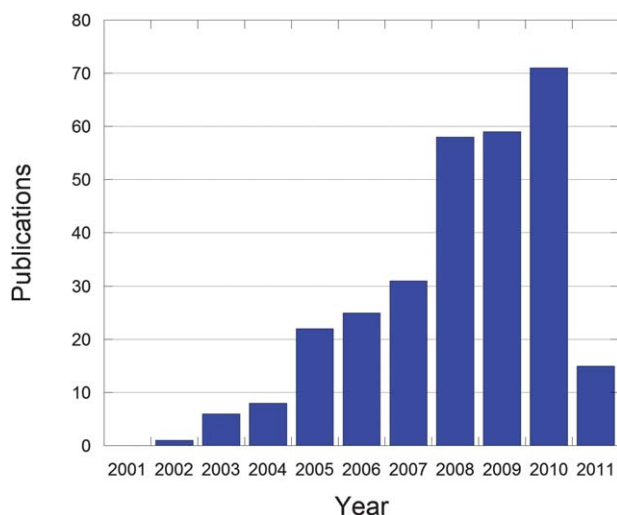
Fig. 1 Publications using PCL electrospun meshes during the last 10 years, until March 2011. Sourced from ISI Web of Knowledge.

Fig. 2 Chemical structures and selected physical properties of common linear polyesters.

room for excitement within the TE electrospinning community, it is important to take stock of where we are and what has been achieved, recognizing the challenges that the technique is yet to overcome.

While electrospinning can be used with different synthetic as well as natural origin polymers,[25,29] this review will focus electrospun materials based on a widely used material, poly-(ε-caprolactone) (PCL). The use of PCL for scaffold fabrication is increasing generally within the TE community, and is one of the more significant polymers electrospun during the past decade (Fig. 1).[30] This review is focused on electrospinning of PCL, synthetic–natural copolymers PCL–collagen or PCL–gelatin and mixtures of PCL with ceramic Ca–P nanoparticles than have reportedly been used for biological applications. Together they make up a small yet significant number of electrospinning articles, and by collating their use within this review, it is anticipated that this forges a clearer path for electrospinning researchers over the next decade of electro-spinning research.

2 State of the art of PCL for TE applications

There has been a gradual increase in the use of PCL for biomaterials and TE.[30] PCL is an aliphatic linear polyester, with a glass transition temperature of $-62\,°C$ and a melting point of 55–$60\,°C$, (Fig. 2) depending on the degree of crystallinity, which in turn is dictated by the molecular weight (normally 3000–100 000 g mol^{-1}) and, to some extent, by the scaffold fabrication process.[31–33] It is biocompatible, bioresorbable and a low-cost synthetic polymer. Due to its semi-crystalline and hydrophobic nature, it exhibits a very slow degradation rate (2–4 years depending on the starting molecular weight) and has mechanical properties suitable for a variety of applications.[31–33] It is a Food and Drug Administration (FDA) approved material and has been clinically used as a slow release drug delivery device and suture material since the 1980s (*i.e.* Capronor®, SynBiosys®, Monocryl® suture).
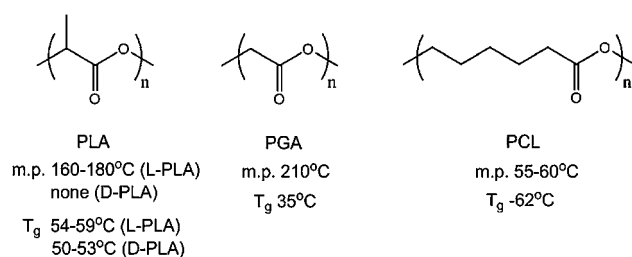
Compared to other aliphatic linear polyesters such as poly-glycolic acid (PGA), polylactic acid (PLA) and the diverse number of copolymer syntheses, PCL has some distinct differences in physical properties that attract researchers. Firstly, PCL does not have isomers in the manner that PLA has. With PLA there are different forms: P*D*LA, P*L*LA, and combinations to form P*DL*LA. Correspondingly the biological degradation and melting points of PLA variants are distinct. The melting point of PCL is substantially lower than PLA, PGA and all of the variant combinations which is most likely a reflection of the greater polarity and potential for hydrogen bonding of PGA and PLA compared with PCL. PCL also has some rheological and visco-elastic properties that allow it to be formed from a wide range of scaffold fabrication technologies. The ease unto which a polymeric material is accommodated into different scaffold fabrication technologies is a property that should not be underestimated. PCL and its copolymers have demonstrated this utility by being successfully used in electrospinning, gravity spinning,[34] phase separation, solid freeform fabrication[35,36] and microparticles,[37,38] in part due to the low melting temperature, very good blend-compatibility, FDA approval and low cost.[30] Other combinations with PCL have been electrospun, such as PCL–PLA[39–43] and PCL–PEG[44] to induce different properties, however, for clarity and conciseness, we will only describe PCL within this review.

One disadvantage of PCL, however, is its hydrophobic nature, resulting in poor wettability, lack of cell attachment and uncontrolled biological interactions with the material.[45] Surfaces with moderate hydrophilicity are able to absorb adequate amount of proteins, while preserving their natural conformation, unlike hydrophobic or very hydrophilic surfaces, which have poor cell attachment.[46–51] In order to rectify this issue, surface modification techniques can alter the chemical and/or physical properties of the surface, by modifying the existing surface or by coating it with a different material. The optimal degree of surface hydrophilicity, however, depends on the cell type and on the specific surface modification method applied.[52] Four main surface modification approaches for PCL include:

• Plasma treatment, which improves the hydrophilicity by forming oxygen-containing groups at the surface.

• Chemical treatment of PCL with a reagent such as sodium hydroxide (NaOH).

• Coating or adsorbing natural ECM proteins, which introduce cell recognition sites for improved cell–biomaterial interaction.

• Blending in biologically active components to provide signals to cellular material.

These approaches towards modifying the surface of PCL elsewhere have all been applied towards electrospun PCL material. Each approach has its strengths and weaknesses, since the various surface modification approaches provide new requirements on the electrospinning process. Electrospun materials can be difficult to handle, especially if their thickness is low, and therefore the surface modification processes can influence the morphology of the structure. This is particularly important for approaches where post-processing is required, in particular when the surface modification requires that the electrospun material is immersed and removed from liquids. The interfacial energies that separate air and liquid can easily damage the morphology and structure of an electrospun material.

2.1 Plasma treatment of electrospun PCL meshes

One approach that avoids immersing electrospun materials into a liquid is the plasma modification process. The main effects of this gaseous route to post-processing are: surface cleaning and etching, which induces changes in topography, and surface reaction between the plasma and surface molecules, which alters the surface charge, surface energy and chemistry, without modifying the bulk properties.[53,54] Using different feed gases such as air, O_2, NH_3, SO_2, CO_2 or other organic compounds, polarized groups such as hydroxyl, carboxyl, amino and sulfate groups can be introduced on PCL surfaces.[46] Plasma treatment using oxygen is commonly used in the biomedical field to increase hydrophilicity of polymers, by increasing the amount of oxygen-containing groups on the surface, mainly hydroxyl (–OH) and carbonyl (–C=O) functionalities.[53–57]

Practically, plasma treatment of electrospun meshes alters the cell–material interactions as observed *in vitro*. Prabhakaran *et al.* showed that Schwann cells exhibited higher proliferation on plasma-treated PCL electrospun meshes than PCL and PCL–collagen meshes, while maintaining their phenotype.[58] Fujihara *et al.* air plasma treated composite PCL–$CaCO_3$ nanofiber meshes before culturing with osteoblasts.[59] Martins *et al.* provided the first systematic study of different plasma treatment conditions (type of gas—Ar or O_2, power—20 or 30 W, exposure time—5 or 10 min) for modification of PCL electrospun nanofiber meshes and influence on the adhesion and proliferation of fibroblasts, chondrocytes and osteoblasts.[55] Undoubtedly more studies on the plasma modification of PCL electrospun scaffolds will follow.

2.2 Chemical treatment of electrospun PCL meshes

Immersing the electrospun meshes into a solution which modifies the surface chemistry has been used for other, non-electrospun, PCL scaffolds.[60] The most common method of chemical treatment is with an aqueous solution of sodium hydroxide (NaOH). This approach introduces hydroxyl groups and side chain modification to the PCL by introduction of carboxylate (–COOH) groups, improving the wettability of the material. The presence of hydroxyl and carboxylate groups decreases the hydrophobicity of the polymer surface due to the slightly

electronegative effects of the carbonyl and hydroxyl functionalities which is also less sterically hindered.

There are tribology effects with NaOH treatment with small pits along the fiber surface. This alters the surface area and changes the interfacial energy as shown by contact angle values. Papers that discuss NaOH treatment papers[61–63] show morphological changes to the fibers as well as surface changes chemically with good characterization data. NaOH treatment has also been used as an intermediate step to produce apatite-covered PCL nanofibers. After immersion in aqueous $CaCl_2$ and $K_2HPO_4 \cdot 3H_2O$, apatite nanocrystals deposited on the NaOH treated surface containing carboxylate groups. The mineralized PCL nanofiber surface was more hydrophilic and stimulated osteogenic differentiation.[64,65]

2.3 Coating of electrospun PCL meshes

Protein adsorption is an important process that dictates the cellular interaction with a material.[66] Therefore PCL meshes are altered by coating processes—either by physical absorption or covalent surface bonding.[67] Some excellent reviews cover the general subject of protein adsorption onto biomaterials surfaces. Such proteins include laminin, gelatin, collagen vitronectin and fibronectin.[46] These proteins interact with the cell, providing signaling cues and adhesion ligands for cell function. For example, laminin has been adsorbed onto the surface of electrospun PCL for promoting neurite outgrowth.[68] While it is also well known that growth factors can also be adsorbed onto surfaces,[69] this has not yet been performed with PCL electrospun fibers.

However to immobilize entities such as growth factors or peptides with biological activity (*e.g.* RGDS peptide from fibronectin), some form of chemical binding needs to be performed. The grafting of hydrophilic polymers onto surfaces has been performed for various biomaterial surfaces, to provide both hydrophilicity and reactive functionalities to conjugate the peptide or protein of interest. Ma *et al.* grafted gelatin on PCL nanofiber meshes to improve endothelial cell spreading and proliferation, and to control cell orientation.[70] They treated the PCL electrospun meshes with air plasma to introduce –COOH groups on the surface and to aid covalent gelatin grafting, using water-soluble carbodiimide as the coupling agent.

2.4 Blending biologically active materials with PCL prior to electrospinning

Since pure electrospun PCL limits cell adhesion, and biological polymers have problems with fiber formation and mechanical integrity in biological media, some researchers have blended both biological polymers and PCL together. For example, despite the cell affinity to natural collagen, electrospun collagen meshes have the disadvantages of poor mechanical strength and that they dissolve in a water-based medium, thus the need for chemical cross-linking, with the consequent possible cytotoxicity problems and mesh morphology changes.[71] Therefore, hybrid PCL–collagen brings together the advantages of synthetic PCL and natural origin collagen. Since collagen denatures to gelatin[72]—also with biological properties—there

This journal is © The Royal Society of Chemistry 2011

J. Mater. Chem., 2011, **21**, 9419–9453 | 9421

have been investigations with gelatin–PCL electrospun material.[70,71,73–76] Finally mixtures of PCL with Ca–P compounds are being investigated for bone TE, owing to the improved mechanical properties and bioactivity, as the Ca–P compounds mimic the mineral crystals present in the natural tissue. PCL-bioactive glass nanofibers have also been investigated.[77,78] The most widely used blends with PCL have been PCL–collagen, PCL–gelatin and PCL–Ca–P electrospun meshes, although there have been others blended with biological molecules including PCL–PLA–gelatin–HA,[79] PCL–PLA–collagen,[80] PCL–chitosan,[81] and PCL–natural human ECM proteins.[82] One important note on blending polymers is that the method does not require post-processing so delicate structures are not affected by liquid immersion, and the samples are rapidly ready for use.

2.5 Factors involved in electrospun meshes for TE studies

A comparative study on recent articles that use PCL or hybrid PCL–collagen, PCL–gelatin and PCL–Ca–P electrospun meshes, for *in vitro* and *in vivo* studies, is presented in Tables 1–7. Only articles with a focus on the different biological assays to monitor cell viability, morphology, adhesion, proliferation, differentiation and infiltration in the mesh were selected for these tables.

It is known that these cellular processes are influenced by the *surface geometry*[83–87] and *curvature*,[88,89] by the *surface chemistry*[90–92] and by the *mechanical properties* of the substrate.[86,93–96] In the context of cell–nanofiber interaction, factors that play an important role in cellular processes are: *fiber diameter*,[97–99] *fiber alignment*,[69,70,76,97,99–101] *elasticity*,[102,103] *pore size distribution and porosity*,[16] *surface topography*,[104] *surface chemistry modification* by coating or adsorbing natural ECM proteins,[68–70] which introduce cell recognition sites for improved cell–biomaterial interaction, or by plasma treatment,[55,58,59,70] which improves the hydrophilicity by forming oxygen-containing groups at the surface.

Since cellular processes are influenced by mesh physical and chemical characteristics, in order to compare biological tests reported on different articles, first the relevant fabrication process parameters (Table 1) and the physical (Table 2) and chemical (Table 3) characterization of the meshes are summarized. The different cell seeding and mesh handling techniques are summarized (Table 4), while *in vitro* (Table 5) and *in vivo* (Table 6) assays are shown.

As it can be seen with the empty entries in Tables 1–7, many of the articles reviewed in this paper do not provide complete information regarding systematic mesh characterization, nor references to previous work, with detailed information of the mesh fabrication process and physical and chemical characteristics of the mesh. Moreover, the fact that different culture medium and cell seeding procedures for the same type of cells are being used, or different assays are performed to measure one same phenomenon—*i.e.* metabolic assays *vs.* DNA content quantification using fluorophores to measure cell proliferation[105]—does not facilitate the comparison of biological tests reported on different articles. It is the purpose of this review to list and discuss the requirements for comprehensive characterization of electrospun meshes and *in vitro* cell culture studies, to enable comparison of results across different laboratories.

3 Requirement for comprehensive characterization of electrospun meshes

In this review we aim to correlate various information compiled on electrospun PCL materials and blends with collagen, gelatin and CaP, from the large number of publications depicted in Fig. 1 (see Tables 1–7). Section 3.1 lists the information required for complete description of the fabrication process, which is necessary for repeatability purposes. Table 1 summarizes the fabrication process parameters employed in the cited publications and reveals gaps in reported data. The physical/chemical characteristics of electrospun meshes and the most suitable characterization techniques are described in Section 3.2. Tables 2 and 3 list corresponding reported data and prove an even stronger evidence of the lack of systematic characterization of the mesh morphology, topography, mechanical properties and chemistry, which play an important role to make the adequate conclusions in *in vitro* studies. In Section 3.3 we discuss issues related to cell and mesh handling and sterilization (Table 4) that are often vaguely described, but are important for replication or to compare results of *in vitro* assays (Table 5) between different groups. Finally, the assessment of electrospun PCL meshes within *in vivo* assays is summarized in Section 3.4 and Table 6.

3.1 Fabrication process

Electrospinning is governed by polymer solution properties, process parameters and ambient conditions and these parameters and effects on the morphology are widely recognized within the electrospinning literature.[16,27,106]

3.1.1 Polymer solution properties. The main polymer solution properties are the polymer type and its molecular weight, solvent type and concentration. Additional properties such as viscosity, surface tension, conductivity and dielectric strength can be useful to relate the electrospinning process parameters (see Section 3.1.2) to the final morphology attained (see Section 3.2.1). Many of these property-relationships are already widespread within the literature; however there are two aspects of polymeric solutions that require attention and also inclusion within electrospinning papers.

The PCL chosen by the vast majority of researchers is sourced from Sigma-Aldrich, with a molecular weight of 80 kDa. Recent discussions with Sigma-Aldrich have revealed that the 80 kDa PCL is currently out of stock, almost worldwide, and replaced with another PCL, this time with a broad molecular weight of 70 to 90 kDa. Therefore while the use of a specific PCL is excellent for standardization and comparative research between groups, the community as a whole is subject to the continued, reproducible, manufacture of PCL. Unfortunately accurately reproducing PCL in such large quantities is technically difficult, and the PCL electrospinning community likely to undergo "readjustment" experiments periodically, and the work published a decade before could become very difficult to precisely reproduce.

Studies with solvents used for electrospinning other polymers show that different solvent conductivities affect the electrospun mesh morphology.[107,108] One particular study was performed for solutions of polystyrene dissolved in dimethyl formamide (DMF).[109] They showed a considerable variability in conductivity, and therefore the morphology of resulting electrospun

9422 | *J. Mater. Chem.*, 2011, **21**, 9419–9453

This journal is © The Royal Society of Chemistry 2011

Table 1 Fabrication process parameters: polymer solution properties, electrospinning process parameters and ambient conditions

Fabrication process	Polymer solution properties		Electrospinning process parameters				Target		Ambient cond.
Ref.	Polymer concentration	Solvent	Voltage/kV	Flow rate/mL h⁻¹	Distance/cm	Needle inner φ	Geometry, dimensions	Rotating speed	
PCL									
Yoshimoto et al.[153]	10 w/v% PCL (80 kDa)	Chloroform	13	6		1 mm	Vertical set up	Stationary	
Li et al.[154]	14 w/v% PCL (80 kDa)	Dimethylformamide (DMF)/tetrahydrofuran (THF) 1:1	12	0.4	20	18 G (0.8 mm)	Vertical set up, Al foil covering Cu plate	Stationary	
Shin et al.[155]	10 w/v% PCL (80 kDa)	Chloroform	13	6		1 mm	Vertical set up,	Stationary	
Shin et al.[156]	10 w/v% PCL (80 kDa)	Chloroform: methanol 1:1	12	6	30	1 mm	Vertical set up, nickel-chrome wire ring, 15 mm ring diam, 0.08 mm wire diam	Stationary	
Ishii et al.[157]	10 w/v% PCL (80 kDa)	Chloroform: methanol 1:1	12	6			Vertical set up, static nickel-chrome wire ring, 15 mm ring diam, 0.08 mm wire diam	Stationary	
Li et al.[148]	14 w/v% PCL (80 kDa)	DMF/THF 1:1	12	0.4	20	18 G (0.8 mm)	Vertical set up, Al foil covering Cu plate	Stationary	
Li et al.[158]	14 w/v% PCL (80 kDa)	DMF/THF 1:1	12	0.4	20	18 G (0.8 mm)	Vertical set up, Al foil covering Cu plate	Stationary	
Pham et al.[16]	8–15 w/v% PCL (80 kDa)	Chloroform: methanol 5:1 to 7:1	19–27	3.5–18	18–33	16–22 G (1.2–0.4 mm)	Horizontal set up	Moves back and forth for uniform coating	
Li et al.[100]	14 w/v% PCL (80 kDa)	DMF/THF 1:1	15		20	18 G (0.8 mm)	Vertical set up, 1 inch Al cylinder	0–7000 rpm = 0–9.3 ms⁻¹	
Kolambkar[159]	13 wt/v% PCL (80 kDa) and coating with GFOGER 20 μg mL⁻¹ 1 h room T	Dichloromethane (DCM)/DMF 40:60	14	0.75	15	22 G (0.4 mm)	Metal cylinder	Stationary and rotating	
Prabhakaran et al.[58]	(1) 12 w/v% PCL (80 kDa) (2) 8 w/v% PCL–collagen (3) Plasma treated p-PCL (vacuum, 30 W, 1 min)	(1) Chloroform: methanol 1:3 (2) HFIP	12	1	12	0.4 mm	15 mm φ coverslips on Al foil target	Stationary	
Nottelet et al.[160]	5–15 w/v% PCL (80 kDa), implant: 15 w/v%	(Acetone), (chloroform/acetone 7:3), chloroform/ethanol 7:3	15–25, implant: 20	12–24, implant: 12	15–25, implant: 20	21 G (0.5 mm)	Stainless steel mandrel with 2 or 4 mm φ, stainless steel plate as a second negative pole	Rotating 4500 rpm and translating 200 moves min⁻¹, 4 cm amplitude	
Pektok et al.[147]	15 w/v% PCL (80 kDa)	Chloroform: ethanol 7:3	20	12	20			Stationary	
Nisbet et al.[161]	10 w/v% PCL, aninolysed in 0.05 M ethylenediamine, in 2-isopropanol	Chloroform: methanol 3:1	20	0.397	15	21 G (0.5 mm)	10 × 10 × 2 cm³ Al container filled with 20 mL PBS	Stationary	
Martins et al.[55]	17 w/v% PCL, plasma treatment: O₂ or Ar, 20 or 30 W, 5 or 10 min, 0.2 mbar	Chloroform: DMF 7:3	9–10	1	20		Al foil	Stationary	

This journal is © The Royal Society of Chemistry 2011

J. Mater. Chem., 2011, **21**, 9419–9453 | 9423

Table 1 (*Contd.*)

Fabrication process	Polymer solution properties		Electrospinning process parameters				Target		Ambient cond.
Ref.	Polymer concentration	Solvent	Voltage/kV	Flow rate/mL h⁻¹	Distance/cm	Needle inner φ	Geometry, dimensions	Rotating speed	
Li et al.[162]	14 w/v% PCL (80 kDa)	DMF/THF 1:1	12		20	18 G (0.8 mm)	Vertical set up, Al foil covering Cu plate	Stationary	
Piskin et al.[163]	40 w/v% PCL (↑M_w 84 kDa: ↓M_w 14 kDa 20:80) Simvastatin loading: (1) Embedding drop 20 μm per scaffold (2) Dispersing in PCL before electrospinning, 20 μm per scaffold	Chloroform: DMF 1:1	15		10		Al foil	Stationary	
Chen et al.[164]	10–20 w/v% PCL (80 kDa)	Acetone	10–25	3	7.5–25	0.8 mm		Stationary	
Nisbet et al.[165]	13 w/v% PCL	Chloroform: methanol 75:25	15	0.6	12	18 G (0.8 mm)	Al rotating mandrel 5 cm φ	200–4000 rpm	
Wise et al.[166]	10 w/v% PCL (80 kDa)	Methylene chloride/ DMF 75:25	1 kV cm⁻¹	1		0.1 mm	Rotating disc	10 ms⁻¹	25 °C, 40%
Lowery et al.[124]	PCL (80 kDa) PCL–PEO (1 × 10⁵ and 2 × 10⁶ g mol⁻¹) and post-H_2O treatment	Chloroform, methanol and DMF	13–37	0.05–0.1	32–48			Stationary	
Ruckh et al.[167]	12 w/v% PCL (80 kDa)	Choroform: methanol 4:1	21	2.8	10	20 G (0.6 mm)	Al foil onto Cu plate	Stationary	
Wu et al.[168]	10 w/v% PCL (80 kDa)	Chloroform: DMF 10:1	18–(−2)	0.4	15	0.8 mm	3.2, 4.5, 7.6 mm diameter cylinder	300 rpm (circumf orientation) 50 rpm (axial orientation) 400–3000 rpm	
Zhu et al.[169]	10–25% PCL (80 kDa) Coated with fibrin	Chloroform: DMF 2:1	15–20	1	10	0.7 mm	Stainless steel plane stand or rotating PCL film		
Cao et al.[170]	(1) 14% PCL (65 kDa) (2) 9.5% PCL (65 kDa)	(1) TFE: dH_2O 5:1 (2) DCM: methanol 3:2	(1) 16–18 (2) 13–15	(1) 1.5 (2) 1.5	(1) 13–14 (2) 8–9	22 G (0.4 mm)		(1) 200–250 (2) 2600–2700	20–23 °C, 51–56%
Jha et al.[171]	50–275 mg mL⁻¹ PCL (65 kDa)	TFE	22–(−4 or −16)	2–20	10–30	18 G (0.8 mm)	Two pole air gap	Stationary	68 °F, 40%
Ye et al.[172]	(1) 16% heparin–PCL (83 kDa) (2) 14% heparin–PCL conjugate with or without FGF2 loading	CH_2Cl_2	20	5	20		Tubular scaffold	Rotating metallic mandrel	
PCL–collagen									
Venugopal et al.[173]	(1) 7.5 w/v% PCL (80 kDa) (2) PCL coated with 10 mg mL⁻¹ collagen (3) 7.5 w/v% collagen (type I)	(1) Chloroform: methanol 3:1 (2 and 3) Hexafluoropropanol (HFP)	13	1	13	27 G (0.21 mm)	Coverslips on Al foil target	Stationary	

This journal is © The Royal Society of Chemistry 2011

Table 1 (*Contd.*)

								Target		
Fabrication process	Polymer solution properties		Electrospinning process parameters							
Ref.	Polymer concentration	Solvent	Voltage/kV	Flow rate/mL h⁻¹	Distance/cm	Needle inner φ		Geometry, dimensions	Rotating speed	Ambient cond.
Venugopal *et al.*[174]	(1) 7.5 w/v% PCL (2) PCL–collagen type I and III 40 : 20 : 10 mg mL⁻¹ (3) Collagen type I and III 80 : 40 mg mL⁻¹	(1) Chloroform : methanol 3 : 1 (2 and 3) HFP	12	0.75	13	27G (0.21 mm)		Coverslips on Al foil target	Stationary	
Venugopal *et al.*[175]	(1) 7.5 w/v% PCL (2) PCL–collagen type I 55 : 25 mg mL⁻¹ (3) Collagen type I 80 mg mL⁻¹	(1) Chloroform : methanol 3 : 1 (2 and 3) HFP	13	(1) 3 (2 and 3) 0.9	13	27 G (0.21 mm)		Coverslips on Al foil target	Stationary	
Schnell *et al.*[152]	(1) 9 w/v% PCL (67 kDa) (2) 9 w/v% PCL (67 kDa)–collagen (type I) 3 : 1	(1) Chloroform : methanol 3 : 1 (2) HFP	20	0.5	20	20 G (0.6 mm)		Fiber alignment using parallel bars 4 cm apart, 12 mm glass coverslips coated with starPEG	Stationary	
Lee *et al.*[176]	5 w/v% PCL–collagen type I 1 : 1, cross-linking in 2.5% glutaraldehyde vapour for 6 h	HFP	20	3	10	18.5 G (0.8 mm)		Stainless steel 4.75 mm φ cylinder	1000 rpm	
Srouji *et al.*[177]	10 w/v% PCL (80 kDa)–collagen type I 1 : 1	DCM : DMF 75 : 25	1 kV cm⁻¹	0.2–0.5	1 kV cm⁻¹	0.5 mm			Stationary	
Choi *et al.*[101]	5 w/v% PCL–collagen (type I) 1 : 1, cross-linking with 2.5% glutaraldehyde vapour for 6 h	HFP	20	3	10	18.5 G (0.8 mm)		Horizontal set up, rotating plate 3.8 × 3.8 × 0.6 cm³	0–3480 rpm	
Chen *et al.*[136]	10 w/v% PCL–2.5 w/v% collagen	HFP–chloroform 3 : 1	10	0.75	15	21 G (0.5 mm)		Vertical set up, connected *via* Teflon tubing	Stationary	
Ekaputra *et al.*[128]	(1) 12.5 w/v% PCL–collagen 4 : 1; (2) Coelectrospinning PCL–collagen and PEO or gelatin (3) Coelectrospinning–coelectrospraying PCL–col and Heprasil	HFP	10	0.75	10	19 G (0.7 mm)		Vertical set up, static and rotating cylinder	100 rpm	
Ekaputra *et al.*[137]	(1) 12.5 w/v% PCL (2) 12.5 w/v% PCL–collagen 4 : 1	HFP : chloroform 4 : 1	10	0.75	15	21 G (0.5 mm)		Al foil	Stationary	
Gerardo-Nava *et al.*[150]	(1) 9 w/v% PCL (65 kDa) (2) 9 w/v% PCL (65 kDa)–collagen (type I) 3 : 1	(1) Chloroform : methanol 3 : 1 (2) HFP	20	0.5	20	20 G (0.6 mm)		Fiber alignment using parallel bars 4 cm apart, 12 mm glass coverslips coated with starPEG	Stationary	

Table 1 (Contd.)

Ref.	Fabrication process — Electrospinning process parameters								
	Polymer solution properties		Voltage/kV	Flow rate/mL h^{-1}	Distance/cm	Needle inner ϕ	Target		Ambient cond.
	Polymer concentration	Solvent					Geometry, dimensions	Rotating speed	
Yang et al.[178]	8 w/v% PCL (80 kDa)–collagen (type I) 3 : 1	HFP	10	0.6	10	0.9 mm	Coverslips or Al foil; cell seeding on mesh, drain DMEM, place 3 cm ring, electrospin onto cells	Stationary	
Powell and Boyce[149]	10 w/v% polymer (1) 100% collagen (2) 1–99% PCL–col (3) 3–97% PCL–col (4) 10–90% PCL–col (5) 30–70% PCL–col (6) 100% PCL PCL (40 kDa)	HFP	25–30				8.5 cm² grounding plate	Stationary	
Tillman et al.[179]	Chemical cross-linking PCL–collagen type I 1 : 1, cross-linking in 2.5% glutaraldehyde vapour for 6 h	HFP	20	3	10	18.5G (0.8 mm)	Stainless steel 4.75 mm ϕ cylinder	1000 rpm	
Ju et al.[180]	5–15 w/v% PCL–collagen type I 1 : 1, cross-linking in 2.5% glutaraldehyde vapour for 6 h	HFP	5–25	1–10	10–20	18 G (0.8 mm)	Stainless steel 4.75 mm ϕ cylinder	1000 rpm	
Szot et al.[181]	5–15 w/v% PCL–collagen type I 1 : 1	HFP	12–(−8)	3	10	18 G (0.8 mm)	15 mm diameter samples	1500 rpm	
PCL–gelatin Zhang et al.[73]	10 w/v% PCL (80 kDa)–gelatin (type A) 1 : 1	TFE				1 mm	Vertical set up, 30 cm Teflon tubing, metal rack with Al foil	Moves back and forth for uniform coating	
Ma et al.[70]	(1) 10 w/v% PCL (80 kDa) (2) p-PCL (air, 30 W, 5 min) (3) p-PCL and gelatin grafting	Chloroform–DMF 70 : 30	15	0.5	15	0.21 mm	Vertical set up, 15 mm coverslips on static and rotating Al cylinder	1000 rpm	
Chong et al.[75]	10 w/v% PCL (80 kDa)–gelatin (type A) 1 : 1	TFE	10.5	0.7		0.4 mm	Vertical set up with Teflon tubing, static 15 × 15 cm collector	Stationary	
Heydarkhan-Hagvall et al.[71]	10 w/v% PCL (10–20 kDa)–gelatin (type B) 1 : 1	HFP	25		15	22 G (0.4 mm)	Vertical set up, Al foil coated with PEG to facilitate removal of mesh	Stationary	
Ghasemi-Mobarakeh et al.[74]	6 w/v% PCL (80 kDa)–gelatin (type A) 50 : 50 and 70 : 30	HFP	12	1		0.4 mm	15 mm coverslips on a rotating disc or Al plate	Stationary and 1000 rpm	

Table 1 (*Contd.*)

| | Electrospinning process parameters | | | | | | Target | | |
| | Polymer solution properties | | | | | | | | |
Ref.	Polymer concentration	Solvent	Voltage/kV	Flow rate/mL h⁻¹	Distance/cm	Needle inner φ	Geometry, dimensions	Rotating speed	Ambient cond.
Gupta et al.[76]	10 w/v% PCL (80 kDa)–gelatin (type A) 1 : 1	TFE	17.5	1.5	13	27 G (0.21 mm)	15 mm coverslips on static and rotating cylinder	4000 rpm	
Lim et al.[182]	6.7 w/v% PCL (65 kDa)–gelatin (type A) 1 : 1	HFP	−26	15	20	20 G (0.6 mm)	7.6 cm × 7.6 cm × 0.2 mm sheet onto glass coated with indium–tin oxide	18 mm coverslips at 1000 rpm	
Tigli et al.[183]	(1) 12 w/v% PCL (80 kDa) (2) 5.4 w/v% PCL–gelatin type A (50 : 50) with and without covalent immobilization of 10 µg mL⁻¹ epidermal growth factor	(1) DCM/DMF 50 : 50 (2) HFP	(1) 25 (2) 12	(1) 12 (2) 1.8	35	0.9 mm	15 mm diameter, 20 µm thick meshes	Stationary	
PCL–CaP compound									
Fujihara et al.[59]	3–7.5 wt/v% PCL (80 kDa)–CaCO₃ nanoparticles (40 nm cubic type) 3 : 1 and 1 : 3, plasma treatment (vacuum, 30 W, 10 min)	Chloroform : methanol 3 : 1	20	1	13	0.21 mm	Vertical set up, 13 mm coverslips on grounded plate	Stationary	Room T, 30–40% humidity
Venugopal et al.[133]	(1) 7.5 w/w% PCL (2) Collagen type I 80 mg mL⁻¹ (3) PCL/nHA (51 nm)/col 60 : 90 : 30 mg mL⁻¹	(1) Chloroform : methanol 3 : 1 (2) HFP (3) HFP	13	1	13		Coverslips on Al foil	Stationary	23 °C, 60% humidity
Wutticharoenmongkol et al.[184]	12 w/v% PCL (80 kDa) PCL—1 w/v% HA (234 ± 68 nm)	DCM/DMF	21	1	10	20 G (0.6 mm)	Al foil wrapped 15 cm φ cylinder	50 rpm	
Erisken et al.[185]	12 w/v% PCL (80 kDa)–0 to 15% βTCP (50 nm–2.5 µm)	DCM	5	0.6	7.5	0.6 mm	Hybrid twin–screw–extrusion/electrospinning	Stationary	
Li et al.[138]	20 w/v% PCL (42.5 kDa)–gelatin coating by layer-by-layer self-assembly-CaP coating by immersion in 10× concentrated SBF	DCM/DMF 80 : 20	15	0.5	15	24 G (0.311 mm)	Al foil	Stationary	
Yu et al.[65]	10 w/v% PCL (80 kDa), surface mineralized with apatite by series of solution treatments	DCM : ethanol 4 : 1	10	0.5	10			Stationary	

This journal is © The Royal Society of Chemistry 2011

J. Mater. Chem., 2011, **21**, 9419–9453 | 9427

Table 1 (*Contd.*)

Ref.	Polymer solution properties		Electrospinning process parameters				Target		Ambient cond.
	Polymer concentration	Solvent	Voltage/kV	Flow rate/mL h^{-1}	Distance/cm	Needle inner ϕ	Geometry, dimensions	Rotating speed	
Yang et al.[132]	12 w/v% PCL (80 kDa)–nHA 1 : 4, 1 : 2	80% TFE in deionized H$_2$O or in PBS	18–22	2	12	0.5 mm	Vertical set up, Teflon tubing	Stationary	
Yang et al.[186]	12 w/v% PCL (80 kDa)–gelatin type A 1 : 1, polymer : nHA 5 : 1	TFE	20	2	8	0.5 mm	Al foil	Stationary	

meshes, between different grades of solvent. Although they investigated only DMF (which is also used in making PCL solutions for electrospinning), the lessons are equally applicable to other solvents used regularly for PCL, namely chloroform, methanol, hexafluoroisopropanol (HFIP), THF, and dichloromethane. The quality and reproducibility of both the polymeric and solvent constituents for electrospinning PCL are a cause for concern and for best results, the brand, grade and preferably lot number of the PCL/solvent should be provided within all publications.

3.1.2 Electrospinning instrument parameters. The potential permutations for the electrospinning instrument parameters are endless and for an electrospun mesh to be reproduced, the following information is required at a minimum (see Table 1): voltage, flow rate, distance needle to collector, vertical or horizontal set up and length of tubing if existing, spinneret inner and outer diameters (can be calculated by providing the gauge size), and type of collector, including dimensions and rotating speed, if any. Such configuration is important for the eventual structure of the electrospun fibers. The polarity of the voltage supply, the location of the ground (if used), and the dimension of the collecting system should all be defined, and also whether the device is enclosed in a housing or exposed to air. In the case of coaxial electrospinning,[110–112] simultaneous deposition of different polymer solutions using multiple spinnerets,[113] use of counter electrodes[114] or multiple field electrospinning apparatus[115] to modify the electrostatic field, electrospinning with dual collection rings,[116,117] electrospinning onto a fluid,[118] ice crystals[119,120] or a hydrogel[121] or any other non-standard set ups, additional information would be required.

3.1.3 Ambient conditions. Electrospinning parameters (solution properties, process parameters and ambient conditions) have an effect on the fiber morphology, which in turn determines mesh properties. This relationship has been described in numerous articles[22,28] and is beyond the scope of this review. However it is important to record ambient temperature and humidity during electrospinning, as they influence the solvent evaporation rate and filament flow dynamics. The challenging aspect of this is that many laboratories do not have accurate climate control environments, and even those with air-conditioning probably do not control humidity levels. The difficult aspect of controlling ambient conditions is that the seasonal effects have a profound influence on various laboratories. Without accurate ambient environmental control, electrospinning performed in the winter should not be directly compared with those in mid-summer. Furthermore it is unlikely that experiments performed during a Canadian winter be accurately reproduced in Thailand during the monsoon season. It is therefore important that laboratories initiate an ambient condition monitoring program, so that the humidity and temperature maxima and minima across seasons are known. Most importantly, the ambient temperature and humidity during electrospinning should be reported in the publication as a range, which is often neglected (see Table 1).

3.2 Characterization of electrospun meshes

3.2.1 Architecture. The bulk architecture of PCL-based non-woven scaffolds is defined by the same parameters as other types

of scaffolds,[107] namely, the fiber diameter, fiber alignment/anisotropy, porosity, pore size, surface area to volume ratio, interconnectivity and tortuosity. The techniques for measuring these parameters are vast and include simple manual or automated image analysis (from SEM, bright field microscopy and TEM), mercury porosimetry, gravimetry, liquid intrusion,[16] gas pycnometry, gas adsorption, and capillary flow porosimetry. The merits of these techniques have been reviewed elsewhere.[122,123]

Other than the fiber diameter, many of the other influential architectural parameters of PCL fibers are commonly overlooked (Table 2) possibly due to the lack of access to appropriate instrumentation which may not be present in all trans-disciplinary laboratories. Pham et al. have offered part of a solution to this problem.[16] In a very comprehensive study in which the PCL fiber diameter and porosity were altered, they found an excellent agreement between the measured pore size using mercury porosimetry and the theoretical values from the fiber diameter (SEM) and the porosity from either gravimetry or liquid intrusion, both of which can be done with simply an analytical balance and can generate statistically similar porosity values between the two methods.[16] They were also able to estimate the pore size from samples with fibers too narrow to withstand the high pressures of mercury porosimetry using this theoretical method. For fibers 4–10 μm in diameter the pore size was 20–45 μm based on mercury porosimetry and theoretical calculations and for 2–3 μm fibers the pore size was approximately 10–15 μm based on only theoretical calculations. The total porosity for all samples was between 83 and 89%. A word of caution is required, however, that when Pham et al. measured their fiber diameter using SEM, to their credit they used five different polymer sheets with five samples taken from each and three measurements made at three different magnifications for a total of 75 measurements per condition. If the fiber diameter is going to be carried through to other theoretical estimates, it needs to be accurate.

Compliant fibrous meshes are, however, susceptible to undergo mechanical deformation under the pressures attained in a mercury porosimetry experiment. Lowery et al. used PCL blended with PEO in order to create fibrous mats with a similar fiber diameter, but different pore diameter, after PEO removal, with the aim of isolating the effect of fiber diameter and pore size on cell growth.[124] The pore size distribution was determined using mercury porosimetry and the results were corrected for the mechanical deformation of the pore size using the algorithm described by Rutledge et al.[125]

In addition to the porosity between fibers, nano-porosity can also manifest itself on the surfaces of PCL fibers produced by co-electrospinning with gelatin or PEO followed by a leaching step.[104,124,126–128] Zhang et al. confirmed additional porosity on PCL fibers after leaching of gelatin using high resolution SEM then measured the increase in porosity using the BET nitrogen gas adsorption method.[104] They observed an increase in BET surface area from 6.56 m^2 g^{-1} to 15.84 m^2 g^{-1} after leaching. This compares with the theoretical surface area of unleached fibers of 3.93 m^2 g^{-1} using the fiber diameter and distribution derived from the SEM using Image J software.

Computerized tomography (CT) is a potential non-destructive method for obtaining the fiber diameter and alignment, porosity, pore size and interconnectivity all from one measurement.[122]

Micro-CT has been used to determine the architecture of PCL/PEG/PLA scaffolds printed using rapid prototyping with 0.5 mm nozzle diameter and for PLGA meshes with 160 μm thick filaments.[122] In each case the porosity, surface area to volume ratio and interconnectivity were calculated from the micro-CT analysis. The resolution of micro-CT is typically down to 6 μm which is too large to be useful for fibers less than approximately 200–1000 nm, however, it is possible that with the recent availability of nano-CT this technique will be used for these types of scaffolds.[129]

3.2.2 Mechanical properties. Accurate measurement of mechanical properties of electrospun meshes for biomedical applications is essential, to guarantee they can withstand the forces during surgical operation and those exerted by physiological activities and/or by tissue growth.

Uniaxial tensile testing gives information about the Young's Modulus or stiffness (E) in tension (slope of the initial linear σ–ε curve), yield strength/strain (σ_y – ε_y) (end of linear elastic region, beginning of non-linear plastic region), fracture stress/deformation (σ_f – ε_f), and fracture energy per volume (area under σ–ε curve) of the nanofiber mesh or single nanofibers. Other techniques such as AFM-based nanoindentation or bending tests have also been reported to measure the local stiffness, hardness and flexural properties. The description of the limitations of these techniques is beyond the scope of this review.

For a tensile test to be accurate and repeatable it is important to report macroscopic dimensions (gauge length and cross-sectional area), the strain rate, the applied load, as well as whether they have been performed at room temperature or under physiological conditions (at 37 °C, in PBS or culture media). Most articles that report mechanical properties of a electrospun mesh measure the cross-sectional area of a highly porous membrane of the order of tens to hundred of microns, using a micrometre with a precision of tens of microns. The error induced by doing so could be one explanation for the large scatter observed in reported mechanical properties of similar composition polymer meshes (Table 2). One alternative could be to take a representative sample of the mesh and to freeze-fracture in liquid nitrogen as depicted in Fig. 3, and to measure the cross-sectional area by image analysis.
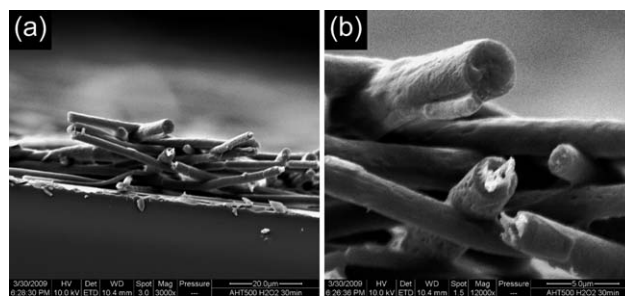
Fig. 3 SEM micrographs of a freeze-fracture cross-section of 10 w/v% PCL–gelatin electrospun mesh (unpublished data), showing the mesh thickness (a) and higher magnification detail (b).

Table 2 Physical characterization of electrospun meshes

| Ref. | Average fiber φ/nm | Degree of fiber alignment | Porosity (and technique)/% | Pore size distribution (and technique)/μm | Mechanical testing | | | | |
					Area/mm²	Thickness/μm	Strain rate/mm min⁻¹	F/N	E/σ_max/ε_max [MPa]/[MPa]/[%]
PCL									
Yoshimoto et al.[153]	400 ± 200					1000			
Li et al.[154]	700				10 × 10	Approx 1000			
Shin et al.[155]					5 × 5	1000			
Shin et al.[156]	250					10			
Ishii et al.[157]	100–5000, average 250					10			
Li et al.[148]	500–900				10 × 10	Approx, 1000			
Li et al.[158]	700				10 × 10	Approx, 1000			
Pham et al.[16]	Alternating micro- and nanofiber layers		83–89 (by mercury porosimetry, liquid intrusion and gravimetry)	20–45 (by mercury porosimetry 0.6–50 psi)					
Li et al.[100]	0 ms⁻¹: 438 ± 156, 9.3 ms⁻¹: 519 ± 127	0 ms⁻¹: 33%, 4.0 ms⁻¹: 71.9%, 9.3 ms⁻¹: 94%			40 × 5	700–1000	2.4	44	E 0 ms⁻¹: 2.1 isotrop, E 4 ms⁻¹: 7.2 (∥), <1 (⊥), E 8 ms⁻¹: 11.6 (∥), <1 (⊥)
Kolambkar[159]	591 ± 199								
Prabhakaran et al.[58]	PCL: 350 ± 83, PCL–col: 245 ± 80					60–70	10		PCL: σ_max = 3.89, ε_max = 101, p-PCL: σ_max = 1.75, ε_max = 97, PCL–col: σ_max = 2, ε_max = 24
Nottelet et al.[160]	200 to 1800, implant: 1900				1 or 3 cm length		10		0.5 < σ_max < 4.2, 100 < ε_max < 600, implant: σ 4.8 MPa, ε 600%
Pektok et al.[147]	1900								σ_max = 4.8, ε_max = 600
Nisbet et al.[161]	750 ± 100					200			
Martins et al.[55]									
Li et al.[162]					8 mm φ	2000			
Piskin et al.[163]	600–800								
Chen et al.[164]	400–1100		~80	56 (400 nm φ), 69 (1100 nm φ) (by SEM)		50			
Nisbet et al.[165]	Rand: 350 ± 125, alig: 450 ± 100	200 rpm: 22%, 4000 rpm: 47%							
Wise et al.[166]	Alig: 492 ± 120, alig: 2796 ± 845								
Lowery et al.[124]	730 ± 90 to 10530 ± 5170		66–87 (by mercury porosimetry)	2.91–38.5 (by mercury porosimetry)		500			
Ruckh et al.[167]	372 ± 179								
Wu et al.[168]	300–500	Circumferencial and axial alignment measured with FTT			5 × 10	0.4	0.25		
Zhu et al.[169]	1–2 μm, some 100 nm								
Cao et al.[170]	(1) 313 ± 5 (2) 506 ± 24		(1) 80.9 (2) 82.6 (by gravimetry)						

9430 | *J. Mater. Chem.*, 2011, **21**, 9419–9453

This journal is © The Royal Society of Chemistry 2011

Table 2 (Contd.)

Ref.	Average fiber φ/nm	Degree of fiber alignment	Porosity (and technique)/%	Pore size distribution (and technique)/μm	Mechanical testing				E/σ_max/ε_max [MPa]/[MPa]/[%]
					Area/mm²	Thickness/μm	Strain rate/mm min⁻¹	F/N	
Jha et al.[171]	400–1500	Highly aligned fibers parallel to cylinder axis measured by 2D FTT	58–95 (liquid intrusion method of Pham[16])		2.67 × 0.295		10		σ_max = 2–4.25 MPa
Ye et al.[172]	(1) PCL: <1 μm (2) Heparin–PCL: 3.5 μm		(1) PCL: 94 (2) Heparin–PCL: 83 (mercury porosimetry)						Burst pressure: (1) PCL: 207 ± 1 kPa (2) PCL–heparin: 208 ± 2 kPa
PCL–collagen									
Venugopal et al.[173]	PCL: 661–700, collagen: 300–375								
Venugopal et al.[174]	PCL–collagen: 210–225 ± 0.035					20			E PCL–collagen: 18
Venugopal et al.[175]	(1) 250 ± 25 (2) 170 ± 75 (3) 275 ± 56			(1) 2.3 (2) 2.2 (3) 2.0		(1) 53.5 (2) 47.3 (3) 45.2			
Schnell et al.[152]	PCL: 559 ± 300, PCL–collagen: 541 ± 164		n/a individual fibers on a substrate						
Lee et al.[176]	PCL: 580 ± 17, PCL–col: 520 ± 14			PCL: 26.9 μm², PCL–col: 22.7 μm² (by SEM)	4.75 mm φ, 12 mm length	300	3, after having immersed samples in PSB at RT for 12 h, (*) also measured suture retention strength, burst pressure strength, compliance and maintenance of tensile prop. in bioreactor after 4 weeks		PCL: E = 7.7, σ_max = 5.1, ε_max = 417, PCL–col (wet): E = 2.7, σ_max = 4, ε_max = 140, PCL–col (dry): E = 3.8, σ_max = 8.3, ε_max = 62
Srouji et al.[177]						100–120			
Choi et al.[101]	Rand: 334 ± 125, alig: 296 ± 97	Histograms of fiber angle as a function of rotation speed			30 × 10	300	30, samples in PBS @ RT for 12 h before test		E_rand: 4.07 (⊥)–4.33 (∥), E_alig: 2.93 (⊥)–4.43 (∥), σ_max rand: 3.86 (⊥)–4.01 (∥), σ_max alig: 3.06 (⊥)–4.88 (∥), ε_max rand: 56.67 (⊥)–53 (∥), ε_max alig: 91.67 (⊥)–42.33 (∥)
Chen et al.[136]	PCL: 564 ± 267; PCL–col: 513 ± 83 with secondary much finer fibers				35 × 10		10, samples in PBS @ 37 °C during testing		PCL: E = 12.35, σ_max = 4.14, ε_max = 147.15, PCL–col: E = 4.5, σ_max = 1.93, ε_max = 187.11
Ekaputra et al.[128]	129 ± 110								

This journal is © The Royal Society of Chemistry 2011

J. Mater. Chem., 2011, **21**, 9419–9453 | 9431

Table 2 (*Contd.*)

Ref.	Average fiber ϕ/nm	Degree of fiber alignment	Porosity (and technique)/%	Pore size distribution (and technique)/μm	Mechanical testing				
					Area/mm²	Thickness/μm	Strain rate/mm min⁻¹	F/N	$E/\sigma\_max/\varepsilon\_max$ [MPa]/[%]
Ekaputra *et al.*[137]	(1) 564 ± 267 (2) 513 ± 83				Tube 6 mm ϕ 2 mm long	1–2 mm wall thickness	2, wet with PBS	225	(1) Mesh only, see Chen[136] (2) Radial direction-compression test PCL–col: $E = 1$, PCL–col&cell sheet: $E = 21.4$, axial direction-indentation PCL–col: $E = 0.61$, PCL–col&cell sheet: $E = 2.4$
Gerardo-Nava *et al.*[150]	PCL: 564.4 ± 208, PCL–collagen: 601.4 ± 151								
Yang *et al.*[178]	455 ± 85					(a) Dermal = 10 layers of fibroblasts, (b) bilayer skin =18 layers of fibroblast, 2 of keratinocytes			
Powell and Boyce[149]	(1) 760 ± 60 (2) 890 ± 100 (3) 630 ± 40 (4) 630 ± 85 (5) 690 ± 30 (6) 200				20 × 4		2	5	(1) $E = 6.7 \times 10^{-3}$ N mm⁻¹, $\sigma\_max = 0.118$, $\varepsilon\_max = 113.7$ (2) $E = 8.4 \times 10^{-3}$ N mm⁻¹, $\sigma\_max = 0.179$, $\varepsilon\_max = 106.4$ (3) $E = 8 \times 10^{-3}$ N mm⁻¹, $\sigma\_max = 0.198$, $\varepsilon\_max = 58.9$ (4) $E = 1.1 \times 10^{-2}$ N mm⁻¹, $\sigma\_max = 0.326$, $\varepsilon\_max = 50.7$ (5) $E = 2.3 \times 10^{-2}$ N mm⁻¹, $\sigma\_max = 0.418$, $\varepsilon\_max = 70.8$ (6) $E = 6 \times 10^{-2}$ N mm⁻¹, $\sigma\_max = 0.974$, $\varepsilon\_max = 102.1$
Tillman *et al.*[179] Ju *et al.*[180]	(1) 270 ± 90 (2) 1000 ± 150 (3) 2390 ± 690 (4) 4450 ± 810			(1) 1.76 ± 1.11 μm² (2) 55.7 ± 34.2 μm² (3) 143.5 ± 80.7 μm² (4) 1199.6 ± 851.2 μm²	8 × 5 Tube 4.75 mm ϕ 12 mm long		5 30, samples in PBS @ RT for 12 h before test	1000 (1) 26 (2) 23 (3) 8 (4) 9	(1) $E = 2.03$, $\sigma\_max = 3.13$, $\varepsilon\_max = 90$ (2) $E = 0.58$, $\sigma\_max = 2.03$, $\varepsilon\_max = 142$ (3) $E = 0.45$, $\sigma\_max = 0.71$, $\varepsilon\_max = 211$ (4) $E = 0.26$, $\sigma\_max = 0.75$, $\varepsilon\_max = 734$
Szot *et al.*[181]	(1) 424 ± 60 (2) 1156 ± 184 (3) 1613 ± 213 (4) 2236 ± 282								

Table 2 (*Contd.*)

Ref.	Average fiber ϕ/nm	Degree of fiber alignment	Porosity (and technique)/%	Pore size distribution (and technique)/μm	Mechanical testing				
					Area/mm²	Thickness/μm	Strain rate/mm min⁻¹	F/N	E/σ_max/ε_max [MPa]/[MPa]/[%]
PCL–gelatin									
Zhang et al.[73]					50 × 10		10	10	PCL: E = 4.98, σ_max = 2.7, ε_max = 126, gel: E = 105, σ_max = 2.5, ε_max = 64, PCL–gel: E = 30.8, σ_max = 1.29, ε_max = 138
Ma et al.[70]	200–1000					25–100			
Chong et al.[75]	470 ± 120		62–75 (by gravimetry)			28			
Heydarkhan-Hagvall et al.[71]	880			Average = 39.25 ± 7.24 (by SEM image analysis)	6	100–200	1		E = 138, σ_max = 11.17
Ghasemi-Mobarakeh et al.[74]	PCL: 431 ± 118, PCL–gelatin 70 : 30: 189 ± 56, PCL–gelatin 50 : 50: 113 ± 33			PCL: 1.7 ± 0.39, PCL–gelatin 70 : 30: 1 ± 0.35, PCL–gelatin 50 : 50: 0.8 ± 0.2 (by capillary flow optometry)	50 × 10		10	10	PCL–gel 70 : 30 higher % elongation but lower strength than PCL
Gupta et al.[76]	PCL rand 471 ± 218; PCL al 200 ± 100; PCL–gel rand 232 ± 194; PCL–gel al 160 ± 86		PCL 86, PCL–gel 90 (by capillary flow porosimeter)	PCL: 1.5, PCL–gel: 1.1–1.25		20–30	5	10	PCL rand: E = 2.5, σ_max = 1.64, ε_max = 80.45, PCL–gel rand: E = 6, σ_max = 1.41, ε_max = 76.51
Lim et al.[182]	(1) As-spun: 570 (2) FS laser-ablated: 660			(1) As-spun: 6.35 (2) FS laser-ablated: 7.45					
Tigli et al.[183]	(1) 488 ± 114 (2) 663 ± 107		(1) 79 (2) 68 (by gravimetry)						
PCL–CaP compound									
Fujihara et al.[59]	PCL: 600 ± 230, PCL–CaCO₃ 1 : 3: 900 ± 450, PCL–CaCO₃ 3 : 1: 760 ± 190				60 × 10		10	10	σ_max PCL only: 4.8; σ_max PCL with 10% CaCO₃: 2.8
Venugopal et al.[133]	From 189 ± 0.026 to 579 ± 272		(1) PCL: 72.3 (2) PCL/nHA: 78.2 (3) PCL/nHA/col: 85.6 (4) Col: 89.7 (by gravimetry)	(1) PCL: 2–15 (2) PCL/nHA: 3–22 (3) PCL/nHA/col: 2–35 (4) Col: 3–50 (by bubble point pressure)	30 × 6		10 @ 25 °C and 74% humidity	10	σ_max: (1) PCL: 2.72 (2) PCL/nHA: 1.25 (3) PCL/nHA/col: 1.73 (4) Col: 1.28
Wutticharoenmongkol et al.[184]	PCL: 950, PCL–HA: 1260					130			

This journal is © The Royal Society of Chemistry 2011

J. Mater. Chem., 2011, **21**, 9419–9453 | 9433

Table 2 (*Contd.*)

| Ref. | Average fiber ϕ/nm | Degree of fiber alignment | Porosity (and technique)/% | Pore size distribution (and technique)/μm | Mechanical testing | | | | $E/\sigma\_max/\varepsilon\_max$ [MPa]/[MPa]/[%] |
					Area/mm²	Thickness/μm	Strain rate/mm min⁻¹	F/N	
Erisken et al.[185]	200–2000 with βTCP varying 0–15%			5–50 (by SEM image analysis)	8.6 mm discs	350–400	(1) Tensile testing: 0.01 mm min⁻¹ @ 25 °C (2) Compression testing: 0.1 mm min⁻¹ with samples in PBS @ 37 °C during testing		(1) Tensile testing, E; PCL: 0.0185; PCL–6% βTCP: 0.0195; PCL–12% βTCP: 0.0275 (2) Compression testing of PCL–15% βTCP, E; unseeded: 0.055; seeded 1 week: 0.065; seeded 4 weeks: 0.110
Li et al.[138]	1200				15 mm discs				
Yu et al.[65]	792 ± 345				10 × 10				
Yang et al.[132]	PCL: 320, PCL–nHA 1:4390, PCL–nHA 1:2: 430			PCL: 1.14 × 0.51, PCL–nHA 1:4: 0.92 × 0.46, PCL–nHA 1:2: 1.61 × 0.69	50 × 10	200–300	10	250	PCL: $E = 6.77$, $\varepsilon\_max = 121$, PCL–nHA 1:4: $E = 19.5$, $\varepsilon\_max = 196$, PCL–nHA 1:2: $E = 13.5$, $\varepsilon\_max = 161$
Yang et al.[186]	(1) PCL–gelatin: 161 nm (2) PCL–gelatin–nHA: 281 nm								

9434 | *J. Mater. Chem.*, 2011, **21**, 9419–9453

This journal is © The Royal Society of Chemistry 2011

3.2.3 Crystallinity. Processing parameters are known to affect the polymer crystallinity. When processing PCL using solution electrospinning the extremely rapid removal of solvent may be expected to result in little opportunity for crystal nucleation and hence poor crystal structure. Competing with this will be the simultaneous drawing of the fibers in the whipping region of the jet to enhance the crystallinity *via* orientation of the polymer chains. The crystallinity of PCL fibers has been studied using several techniques including wide angle X-ray diffraction (WAXD),[130,131] differential scanning calorimetry (DSC)[124,131] and atomic force microscopy (AFM).[131] Electrospinning from dilute solutions results in thinner fibers with higher crystallinity attributed to lower viscosity allowing for better mobility for molecular orientation.[131] The study of a range of fiber diameters found that changes in crystallinity increased linearly from approx. 42% crystallinity for 900 nm PCL fibers to 50% for 250 nm fibers. Likewise, crystallinity further increased when these fibers where stretched after electrospinning.[130] The surface morphology of PCL fibers observed using AFM showed thinner fibers had aligned lamellae within fibrillar structures, whereas the thicker fibers had more misaligned lamellae with respect to the fiber axis suggesting the higher degree of crystallinity in the thinner fibers is a result of orientation.[131]

The effects of enhanced crystallinity of PCL fibers are mainly related to mechanical properties. Increased tensile strength has been reported for PCL fibers below 700 nm which correlates with improved crystallinity and molecular orientation.[130]

3.2.4 Infrared spectroscopy. Fourier Transform Infrared Spectroscopy (FTIR) is a useful and convenient tool for determining the chemical composition of PCL composite fibers. When used with a total internal reflectance (ATR) accessory it provides a quick, semi-quantitative method for confirming the presence of additives to PCL fibers including nano-hydroxyapatite (nHA)[132] and gelatin.[74] The ATR method is normally considered non-destructive, however, good contact between the sample and ATR crystal requires applying significant pressure which will damage delicate scaffold morphologies. The technique is generally considered as being a surface analysis tool as sample depths are typically 0.5–2 μm, however, since most electrospun fibers have diameters in the nanometre to micrometre scales, the spectra obtained will be indicative of the whole fibers, not just the surface. Non-contact reflectance mode is also possible and has been used to identify the individual components of osteoinductive PCL/nHA/collagen fibrous scaffolds including detection of interactions of the nHA with the collagen based on a shift in the collagen carboxyl group from interaction with calcium of the nHA.[133] FTIR is also useful for determining the protein conformation in PCL–gelatin/collagen composites based on characteristic shifts of amide groups indicative of hydrogen bonding.[74,76,133]

Other vibrational spectroscopy techniques such as Raman spectroscopy are also useful in the analysis of nano and microfibrous scaffolds including detection of fiber alignment[134] but to date this technique has not been exploited in the analysis of PCL based fibers.

3.2.5 Surface properties. A change in the contact angle of PCL-based meshes can be a useful indicator of successful surface modification or blending, however, the contact angle is also dependent on the surface roughness and porosity. When a droplet of water is placed on a fibrous mesh only a fraction of the water comes into contact with the fibers which decreases the liquid–solid interactions and increases the liquid–air interactions leading to typically higher contact angles than for smooth surfaces. Tang *et al.*[135] listed contact angles for PCL films, with 105° being the highest values, while Chen *et al.*[136] and Ekaputra *et al.*[137] both reported values of 129° for PCL nanofiber mesh contact angle. In addition, when measuring contact angles of meshes it is often difficult to extrapolate the circular part of the drop profile with the surface when it is irregular. For these reasons the water contact angle of PCL meshes can vary greatly. Table 3 lists reported angles which range from 109° and 134°. The other point to note in Table 3 is that when PCL is modified with collagen,[136,137] gelatin[70,73,74,76,138] or plasma[59] the contact angle reduces to zero meaning it often only serves as a qualitative guide to the success of a modification process when used in this way, although Martins *et al.*[55] have demonstrated how change in contact angle with plasma exposure time can be used to monitor the exposure required.

The simple elemental composition of PCL (C, H and O only) makes it a good substrate for X-ray photoelectron spectroscopy (XPS) which is a highly sensitive surface analysis technique with a small sampling depth relative to fiber diameters. XPS measures the binding energy shifts of inner shell electrons and is commonly used to detect C1s, O1s and N1s shifts. Similarly to contact angle analysis, XPS has been used only relatively qualitatively to identify new chemical species for surface modified PCL including increased oxygen presence after air plasma,[58] increased nitrogen after inclusion of collagen,[58] –OH and –C=O after argon or oxygen plasma.[55]

3.2.6 Degradation properties. Surprisingly, despite the increase in the number of publication describing the use of PCL in electrospinning, very few of them describe the degradation mechanisms and resorption kinetics *in vitro* and/or *in vivo* of PCL electrospun meshes. PCL degradation mainly occurs by hydrolytic cleavage of ester groups,[139,140] which can proceed *via* surface or bulk degradation pathways.[61,62] After an initial linear relationship of ln M_n and time, the second stage begins, which involves loss of mechanical strength and weight.[141] At later stages of *in vivo* degradation, when PCL has broken down into fragments of low molecular weight (M_n < 3000) and high crystallinity, intracellular degradation can take place by phagocytosis.[142] The degradation rate of bulk PCL is rather slow: 2–3 years.[33] Sun *et al.* traced the distribution, absorption and excretion of PCL using radioactive labeling after 3 years in rats.[143]

The degradation mechanisms and kinetics of PCL nanofiber meshes differ from those of bulk PCL, owing to the larger surface area-to-volume ratio, as well as changes in hydrophobicity and crystallinity induced by the electrospinning process.[144] Bölgen *et al.* reported faster degradation kinetics for nanofiber meshes with thinner fibers *in vitro*.[145] PCL nanofiber meshes with an average diameter of 196 nm saw its elongation at break reduced from 82 to 5.7%, the ultimate tensile strength from 17.4 to 5.02 MPa and

This journal is © The Royal Society of Chemistry 2011

J. Mater. Chem., 2011, **21**, 9419–9453 | 9435

Table 3 Chemical characterization of electrospun meshes

Ref.	Contact angle analysis/ degrees	Thermogravimetric analysis (TGA)	Differential scanning calorimetry (DSC)	Gel-permeation chromatography (GPC)	X-Ray diffraction (XRD)	X-Ray photoelectron spectroscopy (XPS)	Fourier transform infrared spectroscopy (FTIR)
PCL							
Kolambkar[159]							FTIR analysis of mineral deposited by cells over a range of 400–2000 cm−1
Prabhakaran et al.[58]	PCL: 122, p-PCL: 0, PCL–col: 65					Proportion O 1s to C 1s of p-PCL greater than PCL, PCL–col contains N 1s peak Minimal difference observed	
Nisbet et al.[161]	Untreated: 36 ± 1 dyn cm−1, treated 42 ± 2 dyn cm−1						
Martins et al.[55]	O₂ 30 W 10 min treatment results in most hydrophilic mesh					C/O ratio decreases with plasma treatment, different treatments lead to different surf. chemistry	
Nisbet et al.[165]	36 ± 2 dyn cm−1		Variation in PCL crystallinity				
Lowery et al.[124]							
PCL–collagen							
Venugopal et al.[174]							FTIR analysis over a range of 400–4000 cm−1
Lee et al.[176]	PCL: 25.4%, PCL–col: 325.1% (by fluid uptake measurement)						
Chen et al.[136]	PCL: 129, PCL–col: 0		Degradation studies: variation in crystallinity	Degradation studies: variation in M_w			
Ekaputra et al.[137]	PCL: 128.68, PCL–col: 0						
PCL–gelatin							
Zhang et al.[73]	Gel: 76.5, PCL: 109, gelatin/PCL: 0						
Ma et al.[70]	PCL: 131, p-PCL: 0, gelatin grafted: 0					Proportion O 1s to C 1s of p-PCL greater than PCL PCL–gel shows N 1s peak	
Ghasemi-Mobarakeh et al.[74]	PCL: 118 ± 6, PCL–gel 70: 30: 32 ± 8, PCL–gel 50 : 50: 0						FTIR analysis over a range of 400–4000 cm−1
Gupta et al.[76]	PCL–gel: 112, PCL–gel: 0						FTIR analysis over a range of 500–4000 cm−1
Lim et al.[182]						Laser machining produced no changes in the surface chemistry	FTIR analysis over a range of 400–4000 cm−1. Laser machining produced no changes in the surface chemistry

9436 | J. Mater. Chem., 2011, **21**, 9419–9453

This journal is © The Royal Society of Chemistry 2011

Table 3 (*Contd.*)

Ref.	Contact angle analysis/degrees	Thermogravimetric analysis (TGA)	Differential scanning calorimetry (DSC)	Gel-permeation chromatography (GPC)	X-Ray diffraction (XRD)	X-Ray photoelectron spectroscopy (XPS)	Fourier transform infrared spectroscopy (FTIR)
Tigli et al.[183]	PCL: 133, PCL–gel: 125, PCL–EGF: 0, PCL–gel–EGF: 0						FTIR analysis over a range of 525–4000 cm⁻¹. EGF successfully immobilized on nanofiber surface
PCL–CaP compound							
Fujihara et al.[59]	PCL: 134, 1 : 3 PCL-CaCO₃: 139, after plasma treatment: 0 for both						
Venugopal et al.[133]					Analysis of crystallographic structure of PCL, PCL/nHA and PCL/nHA/Col		FTIR analysis over a range of 400–4000 cm⁻¹
Erisken et al.[185]	PCL: 133, PCL—15% βTCP: 127	Determine the true content of βTCP in the membrane					
Li et al.[138]	PCL: 117, PCL–gel: 0				Deposited mineral phase mixture of dicalcium phosphate dehydrate and apatite		
Yang et al.[132]		Determine the true content of nHA in the membrane			Analysis of crystallographic structure of the particles		Analysis of chemical structure of the particles and of deposited CaP after 4 days immersed in SBF

This journal is © The Royal Society of Chemistry 2011

J. Mater. Chem., 2011, **21**, 9419–9453 | 9437

the Young's modulus from 3.5 to 1.0 MPa, after 6 months in Ringer solution, at 37 °C and pH 7.4. Fiber with an average diameter of 689 nm on the other hand exhibited a drop from 150 to 122.2% in the elongation at break, from 48.94 to 31.9 MPa in the ultimate strength and from 4.2 to 2.7 MPa in the Young's modulus. Although they observed a slower decrease of M_w compared to solvent-cast PCL film, a 5% decrease *vs.* 29% after 2 months *in vitro*, indicating that the degradation mechanism of PCL nanofibers might shift from bulk degradation to surface degradation. This was also suggested by Kim *et al.*:[146] the diffusion length for the degraded by-products is shorter in small diameter nanofibers, hence the soluble hydrolytic products can easily diffuse into the medium, reducing the risk of autocatalysis in PLA-based electrospun membranes. A shift from the bulk to surface degradation for PCL nanofiber meshes might also explain why Bölgen *et al.* measured a 27% drop in M_w after 90 days *in vivo* compared to a 4% drop *in vitro*,[145] despite similar hydrolytic degradation rates *in vitro* (water at 40 °C) and *in vivo* (rabbits and rats) had been reported for PCL capsules and films after 144 days, concluding that the first stage of degradation was non-enzymatic.[139] The surface-to-volume ratio of the PCL capsules (2 cm length, varying wall thickness) and films (2 × 1 × 0.01 cm³), however, differed only by ten-fold. Johnson *et al.* monitored changes in mechanical properties of PCL electrospun meshes after 7 and 28 days *in vitro* in six different solutions: sodium bicarbonate, sterile saline, pasteurized whole cow milk, bovine urine, bovine plasma and de-ionized water.[103] They observed that material degradation, as well as biological deposition, were responsible for the changes in mechanical properties. Pektok *et al.* investigated the degradation and healing characteristics of 2 mm internal diameter electrospun grafts in rat abdominal aorta.[147] Despite a molecular weight loss of 20% after 24 weeks of implantation, the grafts kept their strength, prevented any aneurysm formation, promoted faster endothelization and premature structural deformation due to degradation seemed not to be a problem.

3.3 Cell and mesh handling prior to *in vitro* assays

It is beyond the scope of the review to discuss all the *in vitro* studies on PCL meshes summarized in Table 5; yet we like to discuss some practical points in this section. Irrespective of the ultimate purpose for the *in vitro* investigations (cell viability, proliferation, differentiation or migration), cell and mesh handling should be thoroughly described for repeatability purposes. While the cell type and origin, type of culture medium and passage number are often included in most articles reporting biological assays, crucial details that allow reproduction of experiments are often omitted. Often this is a result of the researcher not considering the many effects that a protocol could have on their material. One such example is the method of PCL mesh sterilization.

The mesh sterilization methods vary greatly between different laboratories: ethylene oxide, UV radiation or soaking in ethanol. Ethylene oxide is known to soften and plasticize polymers. To the author's knowledge, there are no systematic studies of the UV radiation dose effect on polymer molecular weight and its consequent changes in mechanical and degradation properties.

Regarding the use of ethanol, sterilization is independent of the time immersed in ethanol, and long immersion period is not an optimal sterilization practice.

Furthermore, it has been observed in our group (Fig. 4) that sterilization with ethanol can dramatically change the morphology of PCL–gelatin electrospun meshes. Very few of the referred articles in this review[148,149] analyze the mesh morphology after sterilization and incubation in the culture medium. They do not observe any significant structural degradation on the PCL mesh, after sterilization with UV irradiation only (no ethanol) and 21 days incubation time. Although analysis of mesh morphology changes due to sterilization is most relevant for PCL–collagen or PCL–gelatin meshes. In general, despite the exponential growth of publications describing the use of PCL in tissue engineering, few groups have included a study of the degradation and resorption kinetics.[30] Puppi *et al.* commented that the maintenance of scaffold structure in physiological buffer and the support of cell proliferation/differentiation may be more promising for the engineering of more structurally stable connective tissues.[78]

Regarding cell seeding, although the initial cell seeding density is often reported, the seeding method, that is, the initial seeding volume and whether this is followed by an incubation time for cell attachment before adding the rest of the culture medium, is not always mentioned (see Table 4 and Fig. 5).

Finally, the *in vitro* handling of electrospun meshes is not technically trivial and hence need to be discussed. PCL has a density of 1.13–1.15 g mL⁻¹ and readily sinks, however, nanofibers of this material can be lifted off surfaces from fluid flow. Probably the most destructive aspect of *in vitro* culture to electrospun meshes is the frequent media changes. Removing a liquid entirely, then replacing with another one has strong mechanical effects on the electrospun material, and care is needed in the withdrawal of the fluid so that the sample does not get drawn into the pipette. However the parameters involved in culture are more complicated than this. The mesh could be freely floating in the culture medium, or somehow immobilized onto a surface. The way that an immobilized mesh is achieved, whether it is in direct contact with a substrate underneath or it is suspended between two rings, all has an effect on the results and they are confounded by media changes. Unlike other cell culture protocols, such as protein coating of substrates, cell culture media used and passaging of cells, there are no widely used approach to placing electrospun substrates into a culture well. This is also unlikely to change, as it is one area where researchers are looking at different ways to culture and observe cellular interactions with electrospun fibers.

To demonstrate how the approach of placing electrospun material into a culture well is becoming specialized, a functionally reactive starPEG has been used to pre-treat glass cover slips so that a very low number of fibers can be adhered to a substrate without floating off. In a series of four papers using this approach,[150–152] the reactive PEG macromer adheres the fiber and continues to react with water so that the exposed PEG substrate is non-adhesive to proteins or cells. Fig. 6 shows electrospun PCL/collagen blends collected using a dual beam

9438 | *J. Mater. Chem.*, 2011, **21**, 9419–9453

This journal is © The Royal Society of Chemistry 2011

Table 4 Cell and mesh handling prior to *in vitro* assays

Ref.	Cell type	Culture medium	Seeding density/cells per cm²	Mesh handling	Sterilization
PCL					
Yoshimoto et al.[153]	Rat MSCs	Osteogenic medium, 2 days static culture, then dynamic conditions	Mesh pressed onto cell pellet with 4×10^6 cells	Cut in 10×10 mm²	70% ethanol for 3 h, soaked in purified collagen solution overnight
Li et al.[154]	Fetal bovine chondrocytes, P 2–6	Seeding in 20 µL drops, after 4 h in an incubator, add -Serum-free chondrogenic medium -Serum-containing chondrogenic medium	(1) 1×10^4 (2) 4×10^5	Cut in 10×10 mm², 24-well plates	UV irradiation 30 min, soaked with Hanks' Balanced Salt Solution (HBSS) for 24 h at 37°
Shin et al.[155]	Neonatal Lewis rat bone marrow-derived MSCs	Osteogenic medium, 2 days static culture, then rotating bioreactor	Mesh pressed onto cell pellet with 4×10^6 cells	Cut in 5×5 mm²	70% ethanol for 24 h, soaked in purified collagen solution overnight
Shin et al.[156]	Neonatal Lewis rat cardiomyocytes	40% M-199, 54% Earle's Balanced Salt Solution, 6% FBS	2.5×10^6	Mesh suspended across a nickel-chrome 15 mm ϕ ring (wire 0.08 mm ϕ)	70% ethanol overnight, coating with purified type I collagen solution
Ishii et al.[157]	Neonatal Lewis rat cardiomyocytes	40% M-199, 54% Earle's Balanced Salt Solution, 6% FBS, supplemented with 100 U mL⁻¹ penicillin and streptomycin	2.5×10^6	Mesh suspended across a nickel-chrome 15 mm ϕ ring (wire 0.08 mm ϕ), after days 5–7, up to 5 meshes overlaid in 3D cardiac grafts	
Li et al.[148]	Human bone marrow derived MSCs, P1–3	Seeding in 20 µL drops, after 4 h in an incubator, add chondrogenic medium, supplemented with TGF-β1	4×10^5	Cut in 10×10 mm², 24-well plates	UV irradiation 30 min, soaked with Hanks' Balanced Salt Solution (HBSS) for 24 h at 37°
Li et al.[158]	Human bone marrow derived MSCs	(1) Chondrogenic medium (2) Osteogenic medium (3) Adipogenic medium	(1) 4×10^5 (2 and 3) 2×10^5	Cut in 10×10 mm², 24-well plates	UV irradiation 30 min, soaked with Hanks' Balanced Salt Solution (HBSS) for 24 h at 37°
Pham et al.[16]	Rat MSCs	Osteogenic medium	5×10^5	8 mm discs cut with punch, press fit into cassettes and placed in 6-well plates	Ethylene oxide gas 14 h, 70% ethanol overnight, rinse with PBS 3×, soak with culture the medium in an incubator overnight
Li et al.[100]	Human MSCs, P2	Seeding in 20 µL drops, after 4 h in an incubator, add DMEM, 10% FBS, 1% penicillin/streptomycin/fungizone	250×10^3	Cylinder with 2 or 4 cm length and 2 or 4 mm inner diameter	UV irradiation, prewet with FCS for 30 min
Kolambkar[159]	Human MSCs and amniotic fluid derived SCs	α-MEM, 16.7% FBS and antibiotics, osteogenic medium 4 days after seeding	2×10^4	Cut in 14×14 mm²	
Prabhakaran et al.[58]	Schwann cells, P2	DMEM, 10% FBS, 1% penicillin/ streptomycin/amphotericin-B	1×10^4	24-well plate	
Nottelet et al.[160]				2 mm internal diameter, 13 mm length	γ Radiation 25 kGy
Pektok et al.[147]					γ Radiation 25 kGy
Nisbet et al.[161]	Rat brain derived neural stem cells	(1) 10% FBS (2) Mitogens	5×10^5 cells per mL	Cut in 5×5 mm²	Aminolysed in 0.05 M ethylenediamine, in 2-isopropanol, allowed to react at 20 °C for 10–40 min, washed 3× in ice water, soaked for 1 h in distilled water on ice, dried overnight in a vacuum oven, disinfected with 70% ethanol

Table 4 (*Contd.*)

Ref.	Cell type	Culture medium	Seeding density/cells per cm²	Mesh handling	Sterilization
Martins *et al.*[55]	(1) Mouse lung fibroblasts (2) Human primary osteosarcoma cell line (3) Mouse chondrocyte teratocarcinoma-derived cell line	(1 and 2) DMEM, 10% FBS, 1% antibiotic/antimycotic (3) DMEM-F12, 10% FBS, 2 nM L-glutamine	1 × 10⁵	24-well plate	Ethylene oxide gas
Li *et al.*[162]	Allogenic chondrocytes or xenogenic human MSCs	Seeding in 0.1 mL drops, 20 µL of DMEM, 10% FBS medium added every 30 min, after 2 h seeding on the other side	8 × 10⁵ on each side	Cut in 8 mm discs, 24-well plate	UV irradiation 30 min, soaked in 70% ethanol 30 min, rehydrated with sequential 30 min rinses of 50%, 25%, dH₂O and HBSS
Chen *et al.*[164]	Mouse fibroblasts	Seeding in 1 mL drops, then subjected to vacuum pressure of 2.5, 8 or 20 in Hg. Add DMEM, 10% FCS, 1% penicillin/ streptomycin	3 × 10⁵	Cut in 10 × 10 mm²	Sprayed with alcohol, rinsed twice with PBS, soaked with the culture medium overnight
Nisbet *et al.*[165]				5 mm square scaffolds, rolled into a tube, inserted into a 21 G needle	70% ethanol
Wise *et al.*[166]	Human MSCs, P3	(1) Growth media: DMEM, 15% FBS, 2 mM L-glutamine, 1% antibiotics/ antimycotics (2) Chondrogenic differentiation media	6 × 10⁴	2 cm²	70% ethanol for 1 h, vacuum chamber for 3 days, UV irradiation for 6 h on each side
Lowery *et al.*[124]	Human dermal fibroblasts	DMEM, 10% FBS, 1% penicillin/ streptomycin	(1) Droplet cell seeding: 5 × 10⁵ cells per mL (2) Perfusion cell seeding	2.2 cm diameter	
Ruckh *et al.*[167]	Rat MSCs	DMEM, 10% FBS, 1% penicillin/ streptomycin. On day 7, osteogenic differentiation media	1 × 10⁶	0.7 cm² discs	UV irradiation for 60 min, followed by soaking in 70% ethanol for 60 min, washed 2× with warm PBS, followed by culture media
Wu *et al.*[168]	BAEC cells		5 × 10⁴ cells per well	1.5 × 1.5 cm², meshes held with metal rings	UV radiation for 45 min
Zhu *et al.*[169]	(1) Human umbilical artery smooth muscle cells, P7	(1) Smooth muscle cell basal medium supplemented with human epidermal growth factor (hEGF), insulin, human fibroblastic growth factor-basic (hFGF-B), fetal bovine serum (FBS), and GA-1000	(1) 6 × 10⁴	Small discs	70% ethanol, rinsed with PBS
	(2) Human umbilical vein endothelial cells, P7	(2) Endothelial basal medium supplemented with hydrocortisone, hEGF, FBS, and gentanicin amphotericin B	(2) 10 × 10⁴		
Cao *et al.*[170]	Human primary monocytes	10% autologous serum and macrophage-serum free media	5 × 10⁵ cells onto each scaffold	Discs of 1 cm diameter in 24-well plates	70% ethanol for 30 min, washed 3× with PBS, UV irradiation 30 min
Jha *et al.*[171]	Dorsal root ganglion (DRG) explants from embryonic day 15 rats	Media supplemented with 0.1 µg mL⁻¹ NGF	Single DRG inserted in the cavity	25 G needle used to produce a cavity into the dorsal surface of a tubular scaffold	100% ethanol overnight, rinsed in 70% ethanol, rinsed 3× in sterile PBS
Ye *et al.*[172]	Endothelial cells	DMEM, 10% FBS, 1% penicillin/ streptomycin	(1) 1 × 10⁵ cells mL⁻¹ (2) 1 × 10⁵ cells mL⁻¹ 100 µL into each well	0.5 cm² in 24-well plates	

9440 | *J. Mater. Chem.*, 2011, **21**, 9419–9453

This journal is © The Royal Society of Chemistry 2011

Table 4 (*Contd.*)

Ref.	Cell type	Culture medium	Seeding density/cells per cm²	Mesh handling	Sterilization
PCL–collagen					
Venugopal et al.[173]	Human coronary artery smooth muscle cells, P6 and P7	Smooth muscle basal medium containing 5% FBS and human epidermal growth factors	4×10^4	Mesh on coverslips in 24-well plates	Prewetted in decreasing concentration of ethanol for 24 h, soaked in PBS, soaked in the culture medium overnight
Venugopal et al.[174]	Coronary artery smooth muscle cells, P6 and P7	Smooth muscle basal medium containing 5% FBS	1.5×10^4		
Venugopal et al.[175]	Human dermal fibroblasts		1×10^4	Mesh on coverslips in 24-well plates	Prewetting with decreasing ethanol concentration for 24 h, then soaked in PBS and in the culture medium overnight
Schnell et al.[152]	Dorsal root ganglia neurons, Schwann cells, olfactory ensheathing cells and fibroblasts	DMEM–F12, 10% FCS additional 2 μM forskolin for Schwann cells	2500	Mesh adheres strongly to starPEG treated coverslips, no fibers detaching or floating in 24-well plate	100% ethanol and UV irradiation overnight, washed and prewetted with PBS
Lee et al.[176]	Bovine carotid artery endothelial cells and smooth muscle cells	DMEM, 10% FBS, 1% penicillin/streptomycin	(1) 2×10^4 (2) bEC 1×10^5 inside tube bSMC 5×10^5 outside tube	(1) 10×10 mm² plastic coverslips (2) 4.75 mm $\phi \times 0.3$ mm thick $\times 10$ mm length	Ethylene oxide gas at 30 °C 36 h, soak with the culture medium at 37 °C for 30 min
Srouji et al.[177]	Human bone marrow-derived MSCs	DMEM, 10% FBS, 100 U mL^{-1} penicillin, 100 μg mL^{-1} streptomycin, 2 mM L-glutamine, dynamic flow culture	3×10^4	8 mm ϕ discs in 96-well plates. multilayer construct of $H = 3$ mm, $D = 8$ mm, $d = 0.7$ mm	Oxygen plasma, soaked in the medium for 24 h
Choi et al.[101]	Human skeletal muscle cells, P5	DMEM plus recombinant human epidermal growth factor (rhEGF), insulin, gentamycin, amphotericin, fetuin, dexamethasone, and bovine serum albumin supplemented with 5% FBS	4×10^4	10×10 mm² in 24-well plate, 20×20 mm² in 6-well plate	Ethylene oxide gas at 30 °C 36 h, soak with the culture medium at 37 °C for 30 min
Chen et al.[136]	Rabbit smooth muscle cells	DMEM, 10% FBS, 1% penicillin/streptomycin	(1) 1×10^5 cells per cm² one side only (2) 1×10^6 cells per cm² per side	(1) 15×15 mm², 24-well plate (2) 17×17 mm² clamped between 2 steel rings to culture on both sides, rolled to form a 1.5×5 mm tube sealed with fibrin glue	70% ethanol and UV irradiation, soaked with the culture medium overnight
Ekaputra et al.[128]	Human fetal osteoblasts	DMEM, 10% FCS, 1% antibiotics	1×10^5	8 mm discs in 100 μm cell strainer in 60 mm Petri dishes	Ethanol immersion and UV irradiation, medium conditioning in an incubator overnight
Ekaputra et al.[137]	(1) Pig bone marrow MSCs, P2–3 (2) Wrapped with cell sheet (MSC, osteogenic medium, 2–3 weeks)	(1) DMEM, 10% FBS, 1% antibiotics, w/o osteogenic differentiation factors (2) Osteogenic media, 1 week static, 4 and 8 weeks dynamic culture	(1) 2×10^4 (2) 2×10^4 on both sides	(1) 15×15 (2) 20×20 rolled in tube of 6 mm ϕ	Ethanol, UV irradiation 15 min, soaked with the culture medium overnight
Gerardo-Nava et al.[150]	Human neural progenitor-astrocytes, U373 Astrocytes, SH-SY5Y	Neural Progenitor Differentiation Medium, DMEM/F12 (1 : 1), 10% FBS, 1% penicillin/streptomycin, also SH-SY5Y—retinoic acid @24 h and 5d BDNF	1×10^4 cells per well	Fibers adhered to starPEG treated 12 mm ϕ coverslips, no detaching fibers	70% ethanol and washed 2× with PBS

Table 4 (*Contd.*)

Ref.	Cell type	Culture medium	Seeding density/cells per cm²	Mesh handling	Sterilization
Yang *et al.*[178]	Human epidermal keratinocytes and dermal fibroblasts P4 and P6	DMEM, 10% FBS, 1% penicillin and streptomycin	2 × 10⁴	6 mm discs cut with punch out of multilayer constructs	
Powell and Boyce[149]	Human dermal fibroblasts and epidermal keratinocytes	UCMC 160 medium, air–liquid interface	5 × 10⁵ fibroblasts, incubated 1 day, then 1 × 10⁶ keratinocytes		70% ethanol for 24 h, then rinsed
Tillman *et al.*[179]	(1) Sheep endothelial progenitor cells, P2–4 (2) Sheep primary smooth muscle cells	(1) Endothelial cell growth medium EGM-2 (2) DMEM, 15% FCS	(1) 1 × 10⁶ cells per mL (2) 5 × 10⁵ cells per mL	Cell seeding and conditioning in a bioreactor	
Ju *et al.*[180]	(1) Human aortic smooth muscle cells (external surface) (2) Human aortic endothelial cells (onto the lumen)	(1) DMEM, 10% FBS, 1% penicillin and streptomycin (2) Endothelial cell growth medium EGM-2	(1) 5 × 10⁴ cell per mL (2) 4 × 10⁴ cells per cm²	Tubular scaffold, 12 mm length, 4.75 mm inner diameter	Ethylene oxide gas
Szot *et al.*[181]	(1) Human prostate cancer cell line (PC-3) (2) Murine renal cancer cell line (RENCA) (3) Human breast cancer cell line (MDA-MD-231) (4) Human endothelial cells (HMEC-1)	See in the publication different culture media according to cell line	2 × 10⁴ cells per well (24 well plate)	15 mm diameter	Ethanol, washed in PBS
PCL–gelatin					
Zhang *et al.*[73]	Rabbit bone marrow stromal cells, P2	DMEM, 15% FBS, 100 units mL⁻¹ penicillin, 100 mg mL⁻¹ streptomycin	2 × 10⁴		UV irradiation for 1 h, prewetted with 100% ethanol for 1 h, rinsed 3 × with PBS in 1 h intervals, soaked with the culture medium overnight
Ma *et al.*[70]	Human coronary artery endothelial cells, P9	Endothelial cell basal medium, growth factors (EGM-2), penicillin 100 U mL⁻¹, streptomycin (100 U mL⁻¹)	2.5 μM mL⁻¹, 200 μL per well	24-well plate	75% ethanol
Chong *et al.*[75]	Human dermal fibroblasts, P2–P5	DMEM, 10% FBS, penicillin (100 units mL⁻¹), streptomycin (100 μg mL⁻¹)	1 × 10⁴ cells per well		UV 2 h, 70% ethanol for 24 h, soak with DMEM overnight
Heydarkhan-Hagvall *et al.*[71]	Human adipose-derived SCs, P2	DMEM, 10% FCS, cultured under dynamic conditions	1 × 10⁶	Al foil coated with PEG to facilitate mesh removal	Soaking in 70% ethanol for 20 min, 3 × 5 min rinses with sterile water and PBS
Ghasemi-Mobarakeh *et al.*[74]	Neonatal mouse cerebellum nerve stem cells	DMEM/F12 1 : 1 containing N₂ supplement	1 × 10⁴ cells per well	24-well plate	UV irradiation 2 h, washed 3 × 20 min with PBS, incubated with DMEM/F12 1 : 1 containing N₂ supplement for 24 h
Gupta *et al.*[76]	Rat Schwann cells	DMEM, 10% FCS	6 × 10³	Electrospinning onto 15 mm φ coverslips, placed on 24-well plate and pressed with stainless steel ring	UV irradiation, washed 3× with PBS, immersed in DMEM overnight
Lim *et al.*[182]	Mouse embryonic stem cells	DMEM, 15% FBS, 100 units mL⁻¹ penicillin, 100 mg mL⁻¹ streptomycin, 0.1 mM non-essential amino acids, 10 ng mL⁻¹ LIF, 0.1 mM monothioglycerol, 2 mM L-glutamine, 1 mM sodium pyruvate	5 × 10³ cells per mm²		

This journal is © The Royal Society of Chemistry 2011

Table 4 (*Contd.*)

Ref.	Cell type	Culture medium	Seeding density/cells per cm²	Mesh handling	Sterilization
Tigli et al.[183]	L929 mouse fibroblast	DMEM, 10% FBS	1×10^5 cells per well	24-well plate 15 mm diameter, 20 μm thick meshes	70% ethanol, dried overnight, wetted with PBS
PCL–CaP compound					
Fujihara et al.[59]	Human osteoblasts	DMEM, 10% FBS, 1% penicillin–streptomycin	2.5×10^4	24-well plate	70% ethanol 60 min under UV, rinsed $3\times$ with PBS
Venugopal et al.[133]	Human fetal osteoblasts, P4–5	DMEM/F12 (1 : 1), 10% FBS	2×10^4	24-well plate	
Wutticharoenmongkol et al.[184]	Mouse calvaria-derived pre-osteoblastic cells	MEM, 10% FBS, 1% L-glutamine, 1% penicillin–streptomycin, for some studies, after 5 days, osteogenic media added	3.6×10^4	15 mm discs, 24-well plate, 12 mm φ metal ring placed on top	70% ethanol for 60 min, washed with dH₂O, soaked in the medium overnight
Erisken et al.[185]	Mouse preosteoblast	Minimum essential medium, alpha $1\times$, FBS/penicillin/streptomycin (1/0.1/0.01 vol ratio). After 3 days, MEM α Medium, FBS/penicillin/streptomycin (1/0.1/0.01 vol ratio) and NaHCO₃ (2.2 g L⁻¹)	2×10^4	24-well plate	Multiple immersions into 70% ethanol and PBS solution, soaked with the culture medium
Li et al.[138]	Mouse preosteoblast	α-Minimum essential medium, 10% FBS, 1% penicillin and streptomycin, osteogenic medium for cell culture on meshes	5.7×10^4	24-well plate	70% ethanol overnight, rinsed $3\times$ with PBS
Yu et al.[65]	Murine-derived osteoblastic cells	α-Modified minimum essential medium, 10% FCS, 100 U mL⁻¹ penicillin G sodium, 100 μg mL⁻¹ streptomycin sulfate, 0.25 μg mL⁻¹ amphotericin B, plus osteogenic supplements	2×10^4	24-well plate, sterilized glass ring-type holder to prevent specimens from floating	70% ethanol, drying overnight
Yang et al.[132]	Rat bone marrow cells, P1	α-MEM, 0.5 mg mL⁻¹ gentamycin, 3 μg mL⁻¹ fungizone	2×10^4	24-well plate	70% ethanol for 2 h, washed with PBS $2\times$, soaked in the medium overnight
Yang et al.[186]	Rat dental pulp stem cells	α-MEM supplemented with 10% FCS, 10 mM sodium β-glycerophosphate, 1028 M dexamethasone, L-ascorbic acid (50 μg mL⁻¹), and gentamycin (50 μg mL⁻¹)	5×10^6 cells per mL 1 mL for 6 scaffolds rotating at 6 rpm for 3 h	15 mm discs, 0.3 mm thickness	70% ethanol, rinsed with PBS, soaked in the medium overnight

This journal is © The Royal Society of Chemistry 2011

J. Mater. Chem., 2011, **21**, 9419–9453 | 9443

Table 5 *In vitro* cell culture studies on electrospun meshes

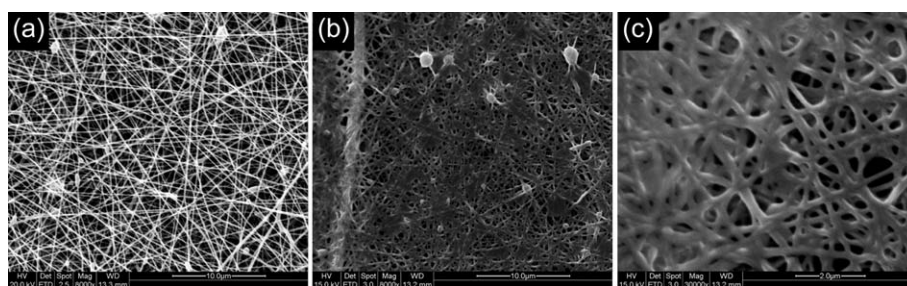| Ref.	Cell viability	Morphology	Proliferation	Differentiation-immunohistochemistry	Histology	Surface migration
PCL Yoshimoto et al.[153]	4 weeks	SEM: after 4 weeks mesh covered with cell multilayers, mineralization and type I collagen formation			Paraffin embedding, 5 μm sections, H&E and Von Kossa's silver nitrate staining for Ca deposits	
Li et al.[154]	21 days	SEM, actin filaments: TRITC-labeled phalloidin, β-tubulin: anti-β-tubulin mouse monoclonal antibody	MTS colorimetric assay: days 0, 7, 14, 21	Collagen type II and IX, aggrecan, COMP, integrins α2, α5, αV, β5	Alcian blue staining	
Shin et al.[156]	Started beating after 3 days, cultured for 14 days	SEM and rhodamine-conjugated phalloidin and DAPI staining		Cardiac troponin I, tropomyosin	Paraffin embedding, 5 μm sections, H&E staining	
Ishii et al.[157]	Between days 5–7, up to 5 meshes overlaid in 3D cardiac grafts, analysis after day 14	SEM and rhodamine-conjugated phalloidin and DAPI staining		Cardiac troponin I, collagen type I and II, presence of gap junctions: anti-connexin43 and anti-mouse IgG antibody	Paraffin embedding, 5 μm sections, H&E and Masson's trichrome staining for collagen assessment	
Li et al.[148]	21 days	SEM	Picogreen dsDNA quantification assay: days 0, 7, 14, 21	Collagen type II, IX and XI and aggrecan, sulfated glycosaminoglycan (sGAG) assay	Paraffin embedding, 10 μm sections, H&E and Alcian blue staining	
Li et al.[158]	21 days	SEM	Picogreen dsDNA quantification assay at 2 and 24 h post-seeding	Cartilage: aggrecan, collagen type II and X, bone: alkaline phosphatase, bone sialoprotein, collagen type Iα2, osteocalcin, adipose: lipoprotein lipase and peroxisome proliferator-activator receptor-g2	Paraffin embedding, 8 μm sections: (1) Cartilage: Alcian blue (2) Bone: Alizarin red, alkaline phosphatase (3) Adipose: Oil Red O and hematoxylin	
Pham et al.[16]	2 h and 24 h	Rhodamine phalloidin staining: cell spreading increased in the presence of nanofibers (stronger F-actin staining)			H&E staining, embedding in Histo-Prep freezing medium and 5 μm frozen sections: cell infiltration hindered with nanofiber layers	
Li et al.[100]	1–28, days FDA/PI live/dead assay	TRITC–phalloidin staining: for rotating speed 0, 4, 8 ms⁻¹, cell pyramidal morphology to more elongated cells, with actin aligned in the direction of the fibers				
Kolambkar et al.[159]	Staining with calcein and ethidium after 1, 7, 14, 28 days		DNA quantification: days 1, 7, 14, 28	Alkaline phosphatase activity: days 1, 7, 14, 28 Arsenazo dye to measure Ca content on day 28		
Prabhakaran et al.[58]	10 days	SEM after 6 days	MTS colorimetric assay: days 2, 4, 6, 8, 10			
Nisbet et al.[161]	7 days			Antibodies for undifferentiated cells, astrocytes, oligodendrocytes and for neurons		
Martins et al.[55]		SEM after 1 day	MTS colorimetric assay: days 1, 3, 7, 14			

9444 | *J. Mater. Chem.*, 2011, **21**, 9419–9453

This journal is © The Royal Society of Chemistry 2011

Table 5 (*Contd.*)

Ref.	Cell viability	Morphology	Proliferation	Differentiation-immunohistochemistry	Histology	Surface migration
Chen et al.[164]	1, 3, 5 days	SEM and SYTOX green fluorescent dye	Detach cells with trypsin–EDTA, counting with hemocytometer		Paraffin embedding, 10 μm sections, H&E stain	
Wise et al.[166]	4, 7, 21, 35 days, live/dead assay		DNA quantification kit			
Lowery et al.[124]	Live/dead assay after day 14	SEM after days 1, 7, 14 and 21, DAPI stain to measure surface cell density and spread of cells across the mesh, after 14 days	Picogreen dsDNA quantification assay: after days 1, 7, 14 and 21	Collagen type II, aggrecan		
Ruckh et al.[167]	Days 1 and 4: MTT assay kit	SEM after 1, 4, 7 days, live cell adhesion using calcein-AM	Cell proliferation up to 7 days	After 3 weeks: alkaline phosphatase activity, calcium and phosphate deposition (EDS), osteopontin, osteocalcin	Calcium content (Alizarin red & von Kossa)	
Wu et al.[168]	4 days	Live cell adhesion using calcein-AM				
Zhu et al.[169]	huSMC viability by mitochondrial function measurement, huECs viability by live/dead assay	SEM, FITC-cell actin, DAPI-cell nuclei		Smooth muscle α-actin (α-SMA) von Willebrand factor (vWF)		
Cao et al.[170]	Days 0, 3, 7, 10	SEM		Neuron specific marker Tubulin J1, counterstained with goat anti-mouse antibody conjugated with Texas red (1 : 200)		
Jha et al.[171]	7–10 days	DAPI stain to reveal nuclei				
Ye et al.[172]	7 days	SEM	ELISA for FGF2 loading efficiency, MTT colorimetric assay after 3, 5 and 7 days			
PCL–collagen						
Venugopal et al.[173]	3 days	SEM	MTS colorimetric assay: days 1, 2, 3	α-Actin cytoskeletal protein		
Venugopal et al.[174]	7 days	SEM after 7 days	MTS colorimetric assay: days 2, 4, 6			
Venugopal et al.[175]	6 days	SEM after 6 days	MTS colorimetric assay: days 2, 4, 6			
Schnell et al.[152]	1–7 days, live/dead assay	SEM	Counting DAPI stained nuclei: 1–7 days	-S100 immunoreactivity for Schwann cells -Neurofilament NF200 for OEC -Mouse monoclonal antibody N0142 for neurons and axons -S100-negative cells for fibroblasts		Migration of DAPI stained nuclei within 200 μm radiating from explant surface
Lee et al.[176]	7 days	SEM and DAPI after 2 days	MTS colorimetric assay: days 1, 3, 7		H&S after 2 days	
Srouji et al.[177]		SEM and confocal mic (CellTrace Far Red DDAO-SE and PI) after 24 h, 6 weeks under dynamic flow culture				

This journal is © The Royal Society of Chemistry 2011

J. Mater. Chem., 2011, **21**, 9419–9453 | 9445

Table 5 (*Contd.*)

Ref.	Cell viability	Morphology	Proliferation	Differentiation-immunohistochemistry	Histology	Surface migration
Choi et al.[101]	7 days	SEM and rhodamine-conjugated phalloidin staining: aligned myotubes with similar ϕ but more than twice the length than those in random mesh	MTS colorimetric assay: days 1, 3, 7. No difference between control, random or aligned mesh	Desmin, myoD, and myosin heavy chain (MHC)		
Chen et al.[136]	(1) 5 weeks (2) 4 weeks		Picogreen dsDNA quantification assay: weeks 1–5		10 μm cryo-cross-sections, H&E and Masson's trichrome staining	
Ekaputra et al.[128]	3 and 10 days, FDA/PI live/dead assay	SEM			10 μm cryo-cross-sections, H&E staining	
Ekaputra et al.[137]	(1) 28 days	SEM after 7 days	Picogreen dsDNA quantification assay: weeks 1, 7, 14, 21, 28	(1) Collagen type I, osteopontin, osteocalcin	(1) 10 μm cryo-cross-sections, H&E, Alizarin red S	
	(2) 4 and 8 weeks			(2) Collagen type I and II, osteocalcin	(2) 10 μm cryo-cross-sections, H&E	
Gerardo-Nava et al.[150]	1, 4 and 7 days	SEM and IHC	Counting DAPI stained nuclei 1, 4 and 7 days	-GFAP and vimentin for hNPac and U373 cells -Neurofilament NF200 for SH-SY5Y		Measurement of distance from pellet of furthers 10% of DAPI stained cells
Yang et al.[178]	1 day, MTT cytotoxicity and live/dead assay	TRITC-conjugated phalloidin and DAPI	CyQuant: days 3, 7, 14		7–10 μm cryo-cross-sections, H&E and DAPI staining	
Powell and Boyce[149]	(1) 28 days (2) 1, 12, 24, 48 and 72 h	Cell migration and infiltration with DAPI, actin cytoskeleton and focal adhesion staining kit	MTT colorimetric assay: days 6, 10, 14; day 10, BrdU to determine active proliferating cells	Day 10 cryosections, human involucrin, human collagen type IV and cellular DNA	Cryosections at days 6, 10, 14, H&E	
Tillman et al.[179]	9 days	SEM, measurement of platelet adhesion		Day 7, anti-PECAM-1 (CD31), anti-von Willebrand factor (vWF) and anti-vascular endothelial (VE)-cadherin antibody	Paraffin embedding, 5 μm sections, H&E stain	
Ju et al.[180]		SEM and phalloidin–DAPI after 4–7 days				
Szot et al.[181]	1, 3, 5, 7 days	SEM				
PCL–gelatin Zhang et al.[73]	1 week	SEM			114 μm penetration, measured by confocal microscopy	
Ma et al.[70]	4 days	SEM and phalloidin–tetramethylrhodamine B isothiocyanate staining	MTS colorimetric assay: days 1, 2, 4	Platelet–endothelial cell adhesion molecule 1 [PECAM-1 or CD31], vascular cell adhesion molecule 1 [VCAM-1 or CD106], intercellular adhesion molecule 1 [ICAM-1 or CD54]		
Chong et al.[75]	(1) Only one side 7 days (2) Both sides, 7 days-flip-7 days	SEM	MTS colorimetric assay: days 1, 3, 5, 7, 14			
Heydarkhan-Hagvall et al.[71]	2 weeks	SEM and DAPI staining	Counting DAPI stained nuclei: 2 weeks		Paraffin embedding, 5 μm sections, H&E staining	

Table 5 (*Contd.*)

Ref.	Cell viability	Morphology	Proliferation	Differentiation-immunohistochemistry	Histology	Surface migration
Ghasemi-Mobarakeh et al.[74]	6 days	SEM after 6 days	MTS colorimetric assay: days 2, 4, 6			
Gupta et al.[76]	9, 12 days	SEM after 9, 12 days	MTS colorimetric assay: days 3, 6, 9. Lower proliferation for aligned fibers			
Lim et al.[182]	1–3 days	SEM and PI staining after 3 days. Cell spreading constrained by FS laser machined cavities	Significant difference in cell density for as-spun and FS laser ablated after 3 days			
Tigli et al.[183]	1, 2, 3, 5, 7 days	SEM and phalloidin–PI staining	MTT colorimetric assay: days after 1, 2, 3, 5 days			
PCL–Ca–P compound						
Fujihara et al.[59]	5 days	SEM after 1, 3, 5 days	MTS colorimetric assay: days 1, 3, 5			
Venugopal et al.[133]	6 days	SEM and staining with 5-chloromethyl fluorescein diacetate after 6 days	MTS colorimetric assay: days 2, 4, 6		Alizarin red staining for Ca deposition	
Wutticharoenmongkol et al.[184]	21 days	SEM after 1, 4, 16, 48 h, SEM after 21 days	MTT colorimetric assay: days 1, 2, 3	Alkaline phosphatase activity. Activity: days 1, 2, 3, 5, 10, osteocalcin expression after days 14 (RT-PCR) and 21 (western blot analysis)	Alizarin red staining for Ca deposition after 14, 21 days	
Erisken et al.[185]	1, 3, 5 days and 4 weeks	Cell staining with methylene blue and polarized light microscopy SEM for tissue constructs	MTT colorimetric assay: days 1, 3, 5	Expression of collagen type-I after 1 week	Paraffin embedding, 5 μm sections, H&E staining, Alizarin red and von Kossa staining for Ca deposition	
Li et al.[138]	7 days	Alexa Fluor1 488 phalloidin staining	MTT colorimetric assay: days 1, 3, 7			
Yu et al.[65]	3 days	SEM after 8 h	MTS colorimetric assay: days 1, 3	Run × 2, collagen type I, alkaline phosphatase and osteocalcin by RT-PCR after 3 days		
Yang et al.[132]		SEM after 4, 16 days	Picogreen dsDNA quantification assay: days 1, 4, 8, 16, 24	Alkaline phosphatase activity: days 1, 4, 8, 16		
Yang et al.[186]	24 days	SEM after 1, 4, 16 days	Picogreen dsDNA quantification assay: days 1, 4, 8, 16, 24	Alkaline phosphatase activity: days 1, 4, 8, 16, 24, osteocalcin expression: days 1, 4, 8, 16, RT-PCR at days 4, 8, 16: osteocalcin (OC), bone sialoprotein (BSP), dentin sialophosphoprotein (Dspp) and dentin matrix protein 1 (Dmp1)		

This journal is © The Royal Society of Chemistry 2011

J. Mater. Chem., 2011, **21**, 9419–9453 | 9447

Fig. 4 SEM micrographs of a random aligned 10 w/v% PCL–gelatin electrospun mesh (unpublished data), before sterilization (a) and same magnification (b) and higher magnification images (c) of the changes in the morphology after sterilization, by soaking with ethanol followed by evaporation.
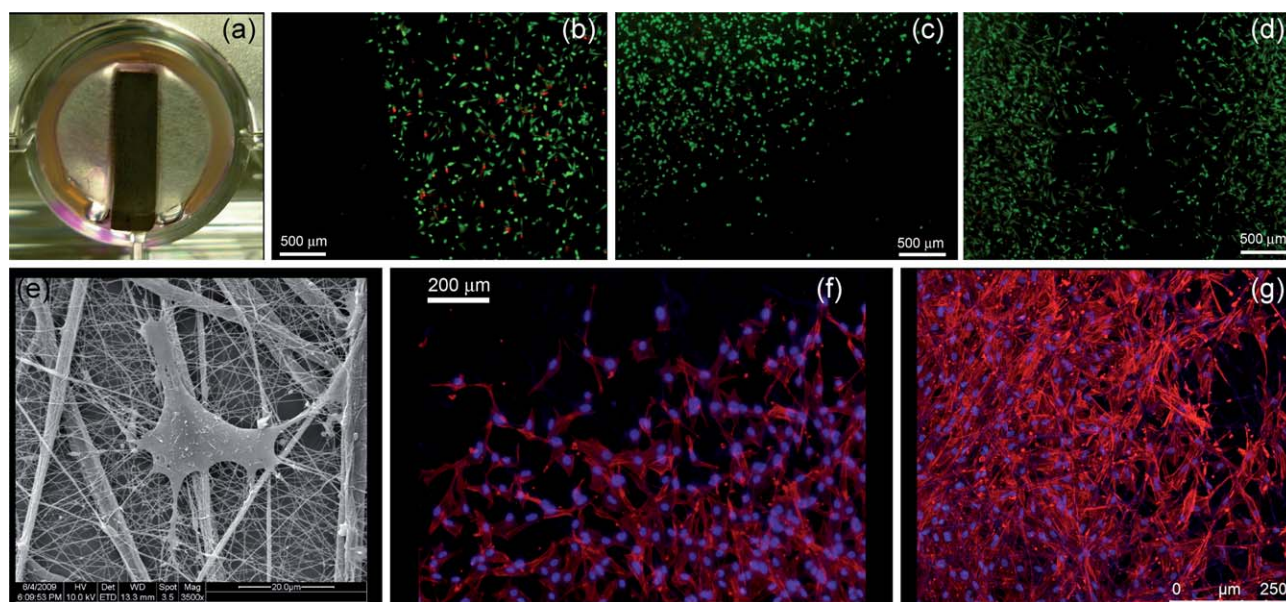

Fig. 5 Scratch test adapted to electrospun meshes for cell migration studies along its surface. Bottom view of a mesh in a 13 mm well plate with a 13 × 3 × 3 mm³ stainless steel strip (a). Osteoblasts were seeded on a random aligned 10 w/v% PCL–gelatin electrospun mesh with a cell seeding density 40 000 cells per cm², in a seeding volume of 50 µL per well, followed by the addition of 250 µL culture medium per well after 1 h incubation time. Live–dead FDA/PI fluorescent micrograph showing a region with high cell density and a 3 mm wide cell free gap, one day after cell seeding, when the metal strip was removed (b), cells migrating into the gap after 3 days (c) and after 7 days (d). SEM image of a cell on a mesh. Fluorescent micrograph (f) and confocal image (g) of phalloidin–DAPI staining of osteoblasts migrating on the edge of the gap after 3 and 7 days respectively (unpublished data).

collector, deposited onto a chemically reactive PEG substrate at a density of 57 ± 7 fibers per mm, resulting in an inter-fiber distance of 17.4 µm. The approach is a highly specialized one and difficult to replicate in other laboratories unless there is access to the starPEG reactive chemical. This macromer is synthesized locally in the laboratory, and there is currently no commercial equivalent available.

Furthermore, there is an increasing interest with depositing electrospun fibers into matrices to perform three-dimensional *in vitro* culture. The choice of matrices, cells, protocols and electrospun fiber properties are likely to be so specific that the experiments performed in such studies will have an even greater array of complexity over current approaches discussed.

3.4 Assessment of electrospun PCL meshes within *in vivo* assays

Considering the extensive use of PCL meshes for *in vitro* studies, there is a surprising lack of literature concerning the *in vivo* implantation of these materials. The studies found are listed in Table 6. One interesting aspect of electrospun PCL material is their (in)compatibility with processes for immunohistochemistry. Paraffin embedding of tissues requires a series of washes within xylene and/or histoclear, which are solvents for PCL. Consequently the preparation of tissues containing electrospun PCL meshes are typically frozen, which removes the need for organic solvents in their preparation. Also important to mention is the methods used to ensure that the mesh has the solvent removed from the material, such as vacuum degassing, so that the solvent

9448 | *J. Mater. Chem.*, 2011, **21**, 9419–9453

This journal is © The Royal Society of Chemistry 2011
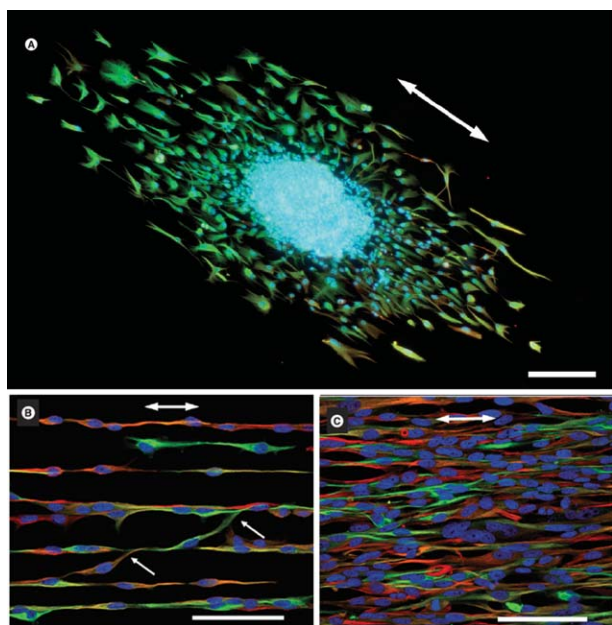
Fig. 6 A pellet of astrocyte driven neural progenitor cells upon a substrate of oriented PLC/collagen electrospun fibers (a). On the same substrates U373 astrocyte cell lines (right) are observed at 4DIV (b) and 7 DIV (c). Adapted from *Nanomedicine* (2009), **4**(1), 11-30 with permission of Future Medicine Ltd

Table 7 Parameters to consider in performing and reporting electrospun PCL fibers

Polymeric parameters
  Molecular weight
  Source; batch/lot number
  Solution properties: source, conductivity
  Polymer solution/melt viscosity; surface tension
Instrument parameters
  Voltage
  Collector–spinneret distance
  Spinneret flow rate
  Electrospinning configuration; vertical or horizontal
  Collector type; dimensions; rotation speed (if applicable)
  Temperature and humidity
Surface treatment methodologies
  Method used; plasma/chemical treatment/adsorbing/blending
  Concentrations of solutions used
  Times for each stage of surface modification
Mesh characterization
  Porosity
  Morphology/architecture (OM/SEM/CT)
  Fiber diameter
  Mechanical properties
  Contact angle
In vitro parameters
  Cell type; passage number
  Media used
  Sterilization method; times for each step
  Assay used
  Mesh anchoring approach
In vivo parameters
  Preparation of samples; method of solvent removal
  Histological fixation method

Table 6 *In vivo* experiments with electrospun meshes

PCL

Shin *et al.*[155]	Implantation in the omenta of rats. After 4 weeks of *in vitro* culture and 4 weeks of implantation: histology (H&S and von Kossa staining), immunohistochemistry (type I collagen) and SEM (multilayers of cells and ECM)
Nottelet *et al.*[160]	Implantation in the abdominal aorta of rats. After 3, 6, and 12 weeks: digital subtraction angiography, to evaluate patency and structural integrity, and histology (H&S stain)
Pektok *et al.*[147]	Implantation in the abdominal aorta of rats. After 3, 6, 12, 18 and 24 weeks: digital subtraction angiography, to evaluate patency and structural integrity, and computed histomorphometry (H&S), to measure endothelial coverage, neointima formation and transmural cellular ingrowth. *In vivo* degradation analysis by changes in molecular weight (M_n and M_w) using size exclusion chromatography
Li *et al.*[162]	*In vivo* iatrogenic, 7 mm ϕ full thickness, articular cartilage repair on femoral condyles in Lee-Sung mini-pigs. After 21 days of *in vitro* culture and 6 months of implantation: mechanical testing (compressive stress relaxation by indentation) and histology (H&E stain)
Piskin *et al.*[163]	Implantation of spiral-wound scaffold, 8 mm ϕ, 2 mm height, in 8 mm ϕ mouse cranial (critical size) defect. After 1, 3 and 6 months implantation (no cell seeding on the mesh): micro-CT and histology (H&S, Goldner's Masson trichrome stain)
Nisbet *et al.*[165]	Implantation in the caudate putamen of rats. Neurite infiltration and inflammation assessed. Immunocytochemistry at days: 1, 3, 7, 14, 21, 28 and 60. Inflammation peaked at day 4 (microglia) and day 7 (astrocytes) and subsided to homeostatic levels by day 60. No evidence of microglial encapsulation. Neurites could penetrate randomly orientated meshes but could not penetrate partially aligned meshes. Neurites grew perpendicular to the direction of fiber alignment at the implant–tissue interface
Cao *et al.*[170]	Subcutaneous implantation in rats to test biocompatibility and host response at weeks 1, 2 and 4. Histology: the thickness of the fibrous capsule around nanofiber meshes is significantly thinner than that around PCL films. Cell infiltration observed in aligned nanofiber meshes; fibrous capsule boundaries found on the surface of random nanofiber meshes and PCL films
Jha *et al.*[171]	Implantation in 10 mm lesions in rodent sciatic nerve (200 mg mL^{-1} PCL, 1 μm diameter fibers, coated with electrosprayed PGA : PLA (50 : 50) to reduce inflammatory cell infiltration). Seven weeks post-implantation revealed dense, parallel arrays of myelinated and non-myelinated axons and functional blood vessels

PCL–collagen

Srouji *et al.*[177]	Subcutaneous implantation in mice. After 6 weeks implantation: SEM and histology (H&S, Masson's trichrome or Toluidine blue stain)
Chen *et al.*[136]	*In vivo* critical size corpus cavernosa defect in male New Zealand white rabbits. Tubular constructs by rolling up double-sided seeded meshes. After 1 and 3 months, histology (H&E stain and Masson's trichrome stain)
Tillman *et al.*[179]	Rabbit aortoiliac bypass model. Mechanical testing of pre-implant graft material and 1 month post-surgery. After 1 month of implantation, CT scanning with intravenous contrast agent and histology (H&E stain)

PCL–Ca–P compound

Yang *et al.*[186]	Subcutaneous implantation into immunocompromised nude mice, 4 and 8 weeks. Histology: scaffolds surrounded by thin fibrous capsule without adverse effects. Cell/scaffold composites showed *in vivo* hard tissue formation. RT-PCR: the combination of nHA in the nanofiber meshes upregulated the expression of specific odontogenic genes

This journal is © The Royal Society of Chemistry 2011

J. Mater. Chem., 2011, **21**, 9419–9453 | 9449

toxicity does not influence the *in vivo* results. The time between manufacture and implantation should be reported.

4 Conclusions

PCL electrospun nanofiber meshes—and its copolymers with collagen or gelatin or mixtures with Ca–P compounds—are currently being investigated in the context of different fields of TE and a broad spectrum of cell types is used for *in vitro* cell cultures studies. The main focus of the articles reviewed in Tables 1–6 is the biological assays. It is, nevertheless, known that the mesh morphology, topography, chemistry and mechanical properties play an important role in cellular processes. It is difficult to compare the results of biological assays reported in different papers, if the information regarding physical and chemical characteristics of the cell environment is incomplete. Physical and chemical characterization of electrospun meshes is not trivial; however, even when the focus of an article is biological, the importance of adequate mesh characterization cannot be underestimated, if we are to compare results reported by different groups. Table 7 summarizes the elements a comprehensive investigation of PCL should include and report. With improved consideration and thorough reporting of such parameters and properties, it will be possible to better compare studies from different laboratories in the future.

Acknowledgements

References

1 J. F. Cooley, *Apparatus for Electrically Dispersing Fluids*, U. P. Office, 1902.
2 W. J. Morton, *Method of Dispersing Fluids*, U. P. Office, 1902.
3 C. L. Norton, *Method of and Apparatus for Producing Fibrous or Filamentary Material*, U. S. P. Office, 1936.
4 A. Formhals, *Process and apparatus for preparing artificial threads*, US Pat. 1975504, 1934.
5 A. Formhals, *Method and apparatus for spinning*, US Pat. 2160962, 1939.
6 A. Formhals, *Artificial thread and method of producing same*, US Pat. 2187306, 1940.
7 A. Formhals, *Method and Apparatus for Spinning*, U. S. P. Office, 1944.
8 D. H. Reneker and I. Chun, Nanometre diameter fibers of polymer, produced by electrospinning, *Nanotechnology*, 1996, **7**(3), 216–223.
9 G. Taylor, Electrically driven jets, *Proc. Natl. Acad. Sci. U. S. A.*, 1969, **A313**(1515), 453–475.
10 D. H. Reneker, et al., Bending instability of electrically charged liquid jets of polymer solutions in electrospinning, *J. Appl. Phys.*, 2000, **87**(9), 4531–4547.
11 A. E. Spivak, Y. A. Dzcnis and D. H. Reneker, A model of steady state jet in the electrospinning process, *Mech. Res. Commun.*, 2000, **27**(1), 37–42.
12 J. M. Deitzel, et al., The effect of processing variables on the morphology of electrospun nanofibers and textiles, *Polymer*, 2001, **42**, 261–272.
13 D. Li and Y. Xia, Electrospinning of nanofibers: reinventing the wheel?, *Adv. Mater.*, 2004, **16**(14), 1151–1170.
14 S. A. Theron, E. Zussman and A. L. Yarin, Experimental investigation of the governing parameters in the electrospinning of polymer solutions, *Polymer*, 2004, **45**, 2017–2030.
15 W. Teo and S. Ramakrishna, A review on electrospinning design and nanofiber assemblies, *Nanotechnology*, 2006, **17**, R89–R106.
16 Q. P. Pham, U. Sharma and A. G. Mikos, Electrospun poly(ε-caprolactone) microfiber and multilayer nanofiber/microfiber scaffolds: characterization of scaffolds and measurement of cellular infiltration, *Biomacromolecules*, 2006, **7**, 2796–2805.
17 C. J. Thompson, et al., Effects of parameters on nanofiber diameter determined from electrospinning model, *Polymer*, 2007, **48**, 6913–6922.
18 T. Han, D. H. Reneker and A. L. Yarin, Buckling of jets in electrospinning, *Polymer*, 2007, **48**, 6064–6076.
19 T. Han, A. L. Yarin and D. H. Reneker, Viscoelastic electrospun jets: initial stresses and elongational rheometry, *Polymer*, 2008, **49**, 1651–1658.
20 T. Han, D. H. Reneker and A. L. Yarin, Pendulum-like motion of straight electrified jets, *Polymer*, 2008, **49**, 2160–2169.
21 D. H. Reneker and A. L. Yarin, Electrospinning jets and polymer nanofibers, *Polymer*, 2008, **49**, 2387–2425.
22 T. J. Sill and H. A. V. Recum, Electrospinning: applications in drug delivery and tissue engineering, *Biomaterials*, 2008, **29**, 1989–2006.
23 J. A. Matthews, et al., Electrospinning of collagen nanofibers, *Biomacromolecules*, 2002, **3**(2), 232–238.
24 W. J. Li, et al., Electrospun nanofibrous structure: a novel scaffold for tissue engineering, *J. Biomed. Mater. Res.*, 2002, **60**(4), 613–621.
25 J. Venugopal, et al., Interaction of cells and nanofiber scaffolds in tissue engineering, *J. Biomed. Mater. Res., Part B*, 2008, **84**(1), 34–48.
26 S. G. Kumbar, et al., Electrospun nanofiber scaffolds: engineering soft tissues, *Biomed. Mater.*, 2008, **3**, 034002, (1–15pp).
27 C. Burger, B. S. Hsiao and A. B. Chu, Nanofibrous materials and their applications, *Annu. Rev. Mater. Res.*, 2006, **36**, 333–368.
28 N. Bhardwaj and S. C. Kundu, Electrospinning: a fascinating fiber fabrication technique, *Biotechnol. Adv.*, 2010, **28**(3), 325–347.
29 Z.-M. Huang, et al., A review on polymer nanofibers by electrospinning and their applications in nanocomposites, *Compos. Sci. Technol.*, 2003, **63**, 2223–2253.
30 M. Woodruff and D. Hutmacher, The return of a forgotten polymer—polycaprolactone in the 21st century, *Prog. Polym. Sci.*, 2010, **35**(10), 1217–1256.
31 I. Engelberg and J. Kohn, Physico-mechanical properties of degradable polymers used in medical applications: a comparative study, *Biomaterials*, 1991, **12**, 292–304.
32 J. C. Middleton and A. J. Tipton, Synthetic biodegradable polymers as orthopedic devices, *Biomaterials*, 2000, **21**(23), 2335–2346.
33 L. S. Nair and C. T. Laurencin, Biodegradable polymers as biomaterials, *Prog. Polym. Sci.*, 2007, **32**, 762–798.
34 M. R. Williamson and A. G. A. Coombes, Gravity spinning of polycaprolactone fibers for applications in tissue engineering, *Biomaterials*, 2004, **25**(3), 459–465.
35 D. W. Hutmacher and S. Cool, Concepts of scaffold-based tissue engineering—the rationale to use solid free-form fabrication techniques, *J. Cell. Mol. Med.*, 2007, **11**(4), 654–669.
36 D. W. Hutmacher, M. Sittinger and M. V. Risbud, Scaffold-based tissue engineering: rationale for computer-aided design and solid free-form fabrication systems, *Trends Biotechnol.*, 2004, **22**(7), 354–362.
37 V. Coccoli, et al., Engineering of poly(ε-caprolactone) microcarriers to modulate protein encapsulation capability and release kinetic, *J. Mater. Sci.: Mater. Med.*, 2008, **19**(4), 1703–1711.
38 A. Luciani, et al., PCL microspheres based functional scaffolds by bottom-up approach with predefined microstructural properties and release profiles, *Biomaterials*, 2008, **29**(36), 4800–4807.
39 I. K. Kwon, S. Kidoaki and T. Matsuda, Electrospun nano- to microfiber fabrics made of biodegradable copolyesters: structural characteristics, mechanical properties and cell adhesion potential, *Biomaterials*, 2005, **26**, 3929–3939.
40 C. M. Vaz, et al., Design of scaffolds for blood vessel tissue engineering using a multi-layering electrospinning technique, *Acta Biomater.*, 2005, **1**, 575–582.
41 X. M. Mo, et al., Electrospun P(LLA-CL) nanofiber: a biomimetic extracellular matrix for smooth muscle cell and endothelial cell proliferation, *Biomaterials*, 2004, **25**, 1883–1890.

9450 | *J. Mater. Chem.*, 2011, **21**, 9419–9453

This journal is © The Royal Society of Chemistry 2011

42 C. Y. Xu, et al., Aligned biodegradable nanofibrous structure: a potential scaffold for blood vessel engineering, *Biomaterials*, 2004, **25**, 877–886.

43 C. Xu, et al., Electrospun nanofiber fabrication as synthetic extracellular matrix and its potential for vascular tissue engineering, *Tissue Eng.*, 2004, **10**(7/8), 1160–1168.

44 D. Grafahrend, et al., Biofunctionalized poly(ethylene glycol)-*block*-poly(ε-caprolactone) nanofibers for tissue engineering, *J. Mater. Sci.: Mater. Med.*, 2008, **19**, 1479–1484.

45 E. S. Place, et al., Synthetic polymer scaffolds for tissue engineering, *Chem. Soc. Rev.*, 2009, **38**, 1139–1151.

46 Z. Ma, Z. Mao and C. Gao, Surface modification and property analysis of biomedical polymers used for tissue engineering, *Colloids Surf., B*, 2007, **60**(2), 137–157.

47 P. B. van Wachem, et al., Interaction of cultured human endothelial cells with polymeric surfaces of different wettabilities, *Biomaterials*, 1985, **6**(6), 403–408.

48 P. B. van Wachem, et al., Adhesion of cultured human endothelial cells onto methacrylate polymers with varying surface wettability and charge, *Biomaterials*, 1987, **8**(5), 323–328.

49 J. H. Lee, et al., Interaction of different types of cells on polymer surfaces with wettability gradient, *J. Colloid Interface Sci.*, 1998, **205**(2), 323–330.

50 J. H. Lee, et al., Interaction of fibroblasts on polycarbonate membrane surfaces with different micropore sizes and hydrophilicity, *J. Biomater. Sci., Polym. Ed.*, 1999, **10**(3), 283–294.

51 E. Tziampazis, J. Kohn and P. V. Moghe, PEG-variant biomaterials as selectively adhesive protein templates: model surfaces for controlled cell adhesion and migration, *Biomaterials*, 2000, **21**(5), 511–520.

52 X. Liu and P. X. Ma, Polymeric scaffolds for bone tissue engineering, *Ann. Biomed. Eng.*, 2004, **32**(3), 477–486.

53 C. M. Chan, T. M. Ko and H. Hiraoka, Polymer surface modification by plasmas and photons, *Surf. Sci. Rep.*, 1996, **24**(1–2), 3–54.

54 P. K. Chu, et al., Plasma-surface modification of biomaterials, *Mater. Sci. Eng., R*, 2002, **36**(5–6), 143–206.

55 A. Martins, et al., Surface modification of electrospun polycaprolactone nanofiber meshes by plasma treatment to enhance biological performance, *Small*, 2009, **5**(10), 1195–1206.

56 J. N. Lai, et al., Study on hydrophilicity of polymer surfaces improved by plasma treatment, *Appl. Surf. Sci.*, 2006, **252**(10), 3375–3379.

57 J. M. Grace and L. J. Gerenser, Plasma treatment of polymers, *J. Dispersion Sci. Technol.*, 2003, **24**(3–4), 305–341.

58 M. P. Prabhakaran, et al., Surface modified electrospun nanofibrous scaffolds for nerve tissue engineering, *Nanotechnology*, 2008, **19**, 455102, (8pp).

59 K. Fujihara, M. Kotaki and S. Ramakrishna, Guided bone regeneration membrane made of polycaprolactone/calcium carbonate composite nano-fibers, *Biomaterials*, 2005, **26**, 4139–4147.

60 M. C. Serrano, et al., Nitric oxide production by endothelial cells derived from blood progenitors cultured on NaOH-treated polycaprolactone films: a biofunctionality study, *Acta Biomater.*, 2009, **5**(6), 2045–2053.

61 C. X. F. Lam, et al., Dynamics of *in vitro* polymer degradation of polycaprolactone-based scaffolds: accelerated *versus* simulated physiological conditions, *Biomed. Mater.*, 2008, **3**, 034108, (15pp).

62 C. X. F. Lam, et al., Evaluation of polycaprolactone scaffold degradation for 6 months *in vitro* and *in vivo*, *J. Biomed. Mater. Res., Part A*, 2008, 906–919.

63 C. X. Lam, S. H. Teoh and D. W. Hutmacher, Comparison of the degradation of polycaprolactone and polycaprolactone–(β-tricalcium phosphate) scaffolds in alkaline medium, *Polym. Int.*, 2007, **56**, 718–728.

64 A. Oyane, et al., Simple surface modification of poly(ε-caprolactone) for apatite deposition from simulated body fluid, *Biomaterials*, 2005, **26**(15), 2407–2413.

65 H.-S. Yu, et al., Apatite-mineralized polycaprolactone nanofibrous web as a bone tissue regeneration substrate, *J. Biomed. Mater. Res., Part A*, 2009, **88**(3), 747–754.

66 J. Goddard and J. Hotchkiss, Polymer surface modification for the attachment of bioactive compounds, *Prog. Polym. Sci.*, 2007, **32**, 698–725.

67 V. Beachley and X. Wen, Polymer nanofibrous structures: fabrication, biofunctionalization, and cell interactions, *Prog. Polym. Sci.*, 2010, **35**(7), 868–892.

68 H. S. Koh, et al., Enhancement of neurite outgrowth using nano-structured scaffolds coupled with laminin, *Biomaterials*, 2008, **29**, 3574–3582.

69 S. Patel, et al., Bioactive nanofibers: synergistic effects of nanotopography and chemical signaling on cell guidance, *Nano Lett.*, 2007, **7**(7), 2122–2128.

70 Z. Ma, et al., Grafting of gelatin on electrospun poly(caprolactone) nanofibers to improve endothelial cell spreading and proliferation and to control cell orientation, *Tissue Eng.*, 2005, **11**(7/8), 1149–1158.

71 S. Heydarkhan-Hagvall, et al., Three-dimensional electrospun ECM-based hybrid scaffolds for cardiovascular tissue engineering, *Biomaterials*, 2008, **29**, 2907–2914.

72 D. I. Zeugolis, et al., Electro-spinning of pure collagen nano-fibers—just an expensive way to make gelatin?, *Biomaterials*, 2008, **29**, 2293–2305.

73 Y. Zhang, et al., Electrospinning of gelatin fibers and gelatin/PCL composite fibrous scaffolds, *J. Biomed. Mater. Res.*, 2005, **72**(1), 156–165.

74 L. Ghasemi-Mobarakeh, et al., Electrospun poly(3-caprolactone)/gelatin nanofibrous scaffolds for nerve tissue engineering, *Biomaterials*, 2008, **29**, 4532–4539.

75 E. J. Chong, et al., Evaluation of electrospun PCL/gelatin nanofibrous scaffold for wound healing and layered dermal reconstitution, *Acta Biomater.*, 2007, **3**, 321–330.

76 D. Gupta, et al., Aligned and random nanofibrous substrate for the *in vitro* culture of Schwann cells for neural tissue engineering, *Acta Biomater.*, 2009, **5**(7), 2560–2569.

77 J.-H. Jo, et al., *In vitro/in vivo* biocompatibility and mechanical properties of bioactive glass nanofiber and poly(ε-caprolactone) composite materials, *J. Biomed. Mater. Res., Part B*, 2009, **91**(1), 213–220.

78 D. Puppi, et al., Polymeric materials for bone and cartilage repair, *Prog. Polym. Sci.*, 2010, **35**, 403–440.

79 D. Gupta, et al., Nanostructured biocomposite substrates by electrospinning and electrospraying for the mineralization of osteoblasts, *Biomaterials*, 2009, **30**, 2085–2094.

80 W. He, et al., Fabrication of collagen-coated biodegradable polymer nanofiber mesh and its potential for endothelial cells growth, *Biomaterials*, 2005, **26**, 7606–7615.

81 M. P. Prabhakaran, et al., Electrospun biocomposite nanofibrous scaffolds for neural tissue engineering, *Tissue Eng. A*, 2008, **14**(11), 1787–1797.

82 K. Schenke-Layland, et al., The use of three-dimensional nanostructures to instruct cells to produce extracellular matrix for regenerative medicine strategies, *Biomaterials*, 2009, **30**(27), 4665–4675.

83 C. S. Chen, et al., Geometric control of cell life and death, *Science*, 1997, **276**, 1425–1428.

84 A. S. G. Curtis and C. D. W. Wilkinson, Reactions of cells to topography, *J. Biomater. Sci., Polym. Ed.*, 1998, **9**(2), 1313–1329.

85 R. McBeath, et al., Cell shape, cytoskeletal tension, and RhoA regulate stem cell lineage commitment, *Dev. Cell*, 2004, **6**, 483–495.

86 V. Vogel and M. Sheetz, Local force and geometry sensing regulate cell functions, *Nat. Rev. Mol. Cell Biol.*, 2006, **7**, 265–275.

87 R. K. Assoian and E. A. Klein, Growth control by intracellular tension and extracellular stiffness, *Trends Cell Biol.*, 2008, **18**(7), 347–352.

88 G. A. Dunn and J. P. Heath, A new hypothesis of contact guidance in tissue cells, *Exp. Cell Res.*, 1976, **101**, 1–14.

89 M. Rumpler, et al., The effect of geometry on three-dimensional tissue growth, *J. R. Soc. Interface*, 2008, **5**, 1173–1180.

90 J. Folkman and A. Moscona, Role of cell shape in growth control, *Nature*, 1978, **273**(5661), 345–349.

91 A. Ben-Ze'ev, S. R. Farmer and S. Penman, Protein synthesis requires cell–surface contact while nuclear events respond to cell shape in anchorage-dependent fibroblasts, *Cell*, 1980, **21**(2), 365–372.

92 B. D. Boyan, et al., Role of material surfaces in regulating bone and cartilage cell response, *Biomaterials*, 1996, **17**(2), 137–146.

93 R. J. Pelham and Y.-L. Wang, Cell locomotion and focal adhesions are regulated by substrate flexibility, *Proc. Natl. Acad. Sci. U. S. A.*, 1997, **94**, 13661–13665.

This journal is © The Royal Society of Chemistry 2011

J. Mater. Chem., 2011, **21**, 9419–9453 | 9451

94 D. E. Discher, P. Janmey and Y.-l. Wang, Tissue cells feel and respond to the stiffness of their substrate, *Science*, 2005, **310**, 1139–1143.

95 T. Yeung, et al., Effects of substrate stiffness on cell morphology, cytoskeletal structure, and adhesion, *Cell Motil. Cytoskeleton*, 2005, **60**, 24–34.

96 A. J. Engler, et al., Matrix elasticity directs stem cell lineage specification, *Cell*, 2006, **126**, 677–689.

97 F. Yang, et al., Electrospinning of nano/microscale poly(L-lactic acid) aligned fibers and their potential in neural tissue engineering, *Biomaterials*, 2005, **26**, 2603–2610.

98 A. S. Badami, et al., Effect of fiber diameter on spreading, proliferation, and differentiation of osteoblastic cells on electrospun poly(lactic acid) substrates, *Biomaterials*, 2006, **27**, 596–606.

99 Y. Liu, et al., Effects of fiber orientation and diameter on the behavior of human dermal fibroblasts on electrospun PMMA scaffolds, *J. Biomed. Mater. Res., Part A*, 2009, **90**(4), 1092–1106.

100 W.-J. Li, et al., Engineering controllable anisotropy in electrospun biodegradable nanofibrous scaffolds for musculoskeletal tissue engineering, *J. Biomech.*, 2007, **40**, 1686–1693.

101 J. S. Choi, et al., The influence of electrospun aligned poly(ε-caprolactone)/collagen nanofiber meshes on the formation of self-aligned skeletal muscle myotubes, *Biomaterials*, 2008, 2899–2906.

102 J. Lee, et al., The effect of gelatin incorporation into electrospun poly(L-lactide-*co*-epsilon-caprolactone) fibers on mechanical properties and cytocompatibility, *Biomaterials*, 2008, **29**(12), 1872–1879.

103 J. Johnson, et al., Electrospun PCL *in vitro*: a microstructural basis for mechanical property changes, *J. Biomater. Sci., Polym. Ed.*, 2009, **20**(4), 467–481.

104 Y. Z. Zhang, et al., Fabrication of porous electrospun nanofibers, *Nanotechnology*, 2006, **17**, 901–908.

105 V. M. Quent, et al., Discrepancies between metabolic activity and DNA content as tool to assess cell proliferation in cancer research, *J. Cell. Mol. Med.*, 2010, **14**(4), 1003–1013.

106 A. Martins, R. L. Reis and N. M. Neves, Electrospinning: processing technique for tissue engineering scaffolding, *Int. Mater. Rev.*, 2008, **53**(5), 257–274.

107 T. Lin, et al., The charge effect of cationic surfactants on the elimination of fiber beads in the electrospinning of polystyrene, *Nanotechnology*, 2004, **15**(9), 1375–1381.

108 J. F. Zheng, et al., Studies on the controlled morphology and wettability of polystyrene surfaces by electrospinning or electrospraying, *Polymer*, 2006, **47**(20), 7095–7102.

109 T. Uyar and F. Besenbacher, Electrospinning of uniform polystyrene fibers: the effect of solvent conductivity, *Polymer*, 2008, **49**(24), 5336–5343.

110 Y. Lu, et al., Mild immobilization of diverse macromolecular bioactive agents onto multifunctional fibrous membranes prepared by coaxial electrospinning, *Acta Biomater.*, 2009, **5**(5), 1562–1574.

111 Y. Z. Zhang, et al., Characterization of the surface biocompatibility of the electrospun PCL–collagen nanofibers using fibroblasts, *Biomacromolecules*, 2005, **6**(5), 2583–2589.

112 P. Zhao, et al., Biodegradable fibrous scaffolds composed of gelatin coated poly(ε-caprolactone) prepared by coaxial electrospinning, *J. Biomed. Mater. Res., Part A*, 2007, **83**(2), 372–382.

113 S. Kidoaki, I. K. Kwon and T. Matsuda, Mesoscopic spatial designs of nano- and microfiber meshes for tissue-engineering matrix and scaffold based on newly devised multilayering and mixing electrospinning techniques, *Biomaterials*, 2005, **26**(1), 37–46.

114 L. S. Carnell, et al., Aligned mats from electrospun single fibers, *Macromolecules*, 2008, **41**, 5345–5349.

115 J. M. Deitzel, et al., Controlled deposition of electrospun poly(ethylene oxide) fibers, *Polymer*, 2001, **42**, 8163–8170.

116 P. D. Dalton, D. Klee and M. Möller, Electrospinning with dual collection rings, *Polymer*, 2005, **46**, 611–614.

117 M. Acharya, G. K. Arumugam and P. A. Heiden, Dual electric field induced alignment of electrospun nanofibers, *Macromol. Mater. Eng.*, 2008, **293**, 666–674.

118 R. Tzezana, E. Zussman and S. Levenberg, A layered ultra-porous scaffold for tissue engineering, created *via* a hydrospinning method, *Tissue Eng., Part C*, 2008, **14**(4), 281–288.

119 O. D. Schneider, et al., Cotton wool-like nanocomposite biomaterials prepared by electrospinning: *in vitro* bioactivity and osteogenic differentiation of human mesenchymal stem cells, *J. Biomed. Mater. Res., Part B*, 2008, **84**(2), 350–362.

120 M. Simonet, et al., Ultraporous 3D polymer meshes by low-temperature electrospinning: use of ice crystals as a removable void template, *Polym. Eng. Sci.*, 2007, **47**(12), 2020–2026.

121 K. D. Anderson, et al., Hydrogel microstructures combined with electrospun fibers and photopatterning for shape and modulus control, *Polymer*, 2008, **49**, 5284–5293.

122 S. T. Ho and D. W. Hutmacher, A comparison of micro-CT with other techniques used in the characterization of scaffolds, *Biomaterials*, 2006, **27**, 1362–1376.

123 D. R. Nisbet, et al., Surface and bulk characterization of electrospun membranes: problems and improvements, *Colloids Surf., B*, 2009, **71**(1), 1–12.

124 J. L. Lowery, N. Datta and G. C. Rutledge, Effect of fiber diameter, pore size and seeding method on growth of human dermal fibroblasts in electrospun poly(ε-caprolactone) fibrous mats, *Biomaterials*, 2010, **31**(3), 491–504.

125 G. C. Rutledge, J. L. Lowery and C. L. Pai, Characterization by mercury porosimetry of non-woven fiber media with deformation, *J. Eng. Fibers Fabr.*, 2009, **4**(3), 1–13.

126 B. M. Baker, et al., The potential to improve cell infiltration in composite fiber-aligned electrospun scaffolds by the selective removal of sacrificial fibers, *Biomaterials*, 2008, **29**(15), 2348–2358.

127 B. M. Baker, et al., Fabrication and modeling of dynamic multipolymer nanofibrous scaffolds, *J. Biomech. Eng.*, 2009, **131**(10), 101012.

128 A. K. Ekaputra, et al., Combining electrospun scaffolds with electrosprayed hydrogels leads to three-dimensional cellularization of hybrid constructs, *Biomacromolecules*, 2008, **9**, 2097–2103.

129 B. Marelli, et al., Compliant electrospun silk fibroin tubes for small vessel bypass grafting, *Acta Biomater.*, 2010, **6**(10), 4019–4026.

130 S. C. Wong, A. Baji and S. W. Leng, Effect of fiber diameter on tensile properties of electrospun poly(ε-caprolactone), *Polymer*, 2008, **49**(21), 4713–4722.

131 C. T. Lim, E. P. S. Tan and S. Y. Ng, Effects of crystalline morphology on the tensile properties of electrospun polymer nanofibers, *Appl. Phys. Lett.*, 2008, **92**(14), 141908.

132 F. Yang, et al., Development of an electrospun nano-apatite/PCL composite membrane for GTR/GBR application, *Acta Biomater.*, 2009, **5**(9), 3295–3304.

133 J. Venugopal, et al., Biocomposite nanofibers and osteoblasts for bone tissue engineering, *Nanotechnology*, 2007, **18**, 055101, (8pp).

134 M. Lisunova, et al., Nanofibers of CA/PAN with high amount of carbon nanotubes by core–shell electrospinning, *Compos. Sci. Technol.*, 2010, **70**(11), 1584–1588.

135 Z. G. Tang, et al., Surface properties and biocompatibility of solvent-cast poly(ε-caprolactone) films, *Biomaterials*, 2004, **25**(19), 4741–4748.

136 Z. C. C. Chen, et al., *In vitro* and *in vivo* analysis of co-electrospun scaffolds made of medical grade poly(ε-caprolactone) and porcine collagen, *J. Biomater. Sci., Polym. Ed.*, 2008, **19**(5), 693–707.

137 A. K. Ekaputra, et al., Composite electrospun scaffolds for engineering tubular bone grafts, *Tissue Eng. A*, 2009, **15**(12), 3779–3788.

138 X. Li, et al., Coating electrospun poly(ε-caprolactone) fibers with gelatin and calcium phosphate and their use as biomimetic scaffolds for bone tissue engineering, *Langmuir*, 2008, **24**, 14145–14150.

139 C. G. Pitt, et al., Aliphatic polyesters. 1. The degradation of poly(ε-caprolactone) *in vivo*, *J. Appl. Polym. Sci.*, 1981, **26**(11), 3779–3787.

140 S. A. Ali, et al., Mechanisms of polymer degradation in implantable devices. I. Poly(caprolactone), *Biomaterials*, 1993, **14**(9), 648–656.

141 C. G. Pitt, et al., Aliphatic polyesters. 2. The degradation of poly(D, L-lactide), poly(ε-caprolactone), and their copolymers *in vivo*, *Biomaterials*, 1981, **2**(4), 215–220.

142 S. C. Woodward, et al., The intracellular degradation of poly(ε-caprolactone), *J. Biomed. Mater. Res.*, 1985, **19**(4), 437–444.

143 H. Sun, et al., The *in vivo* degradation, absorption and excretion of PCL-based implant, *Biomaterials*, 2006, **27**(9), 1735–1740.

144 Y. Dong, et al., Degradation behaviors of electrospun resorbable polyester nanofibers, *Tissue Eng., Part B: Rev.*, 2009, **15**(3), 333–351.

145 N. Bölgen, et al., *In vitro* and *in vivo* degradation of non-woven materials made of poly(ε-caprolactone) nanofibers prepared by electrospinning under different conditions, *J. Biomater. Sci., Polym. Ed.*, 2005, **16**(12), 1537–1555.

9452 | *J. Mater. Chem.*, 2011, **21**, 9419–9453

This journal is © The Royal Society of Chemistry 2011

146 K. Kim, et al., Control of degradation rate and hydrophilicity in electrospun non-woven poly(D,L-lactide) nanofiber scaffolds for biomedical applications, *Biomaterials*, 2003, **24**(27), 4977–4985.

147 E. Pektok, et al., Degradation and healing characteristics of small-diameter poly(ε-caprolactone) vascular grafts in the rat systemic arterial circulation, *Circulation*, 2008, **118**(24), 2563–2570.

148 W.-J. Li, et al., A three-dimensional nanofibrous scaffold for cartilage tissue engineering using human mesenchymal stem cells, *Biomaterials*, 2005, **26**, 599–609.

149 H. M. Powell and S. T. Boyce, Engineered human skin fabricated using electrospun collagen–PCL blends: morphogenesis and mechanical properties, *Tissue Eng. A*, 2009, **15**(8), 2177–2187.

150 J. Gerardo-Nava, et al., Human neural cell interactions with orientated electrospun nanofibers in vitro, *Nanomedicine*, 2009, **4**(1), 11–30.

151 K. Klinkhammer, et al., Deposition of electrospun fibers on reactive substrates for in vitro investigations, *Tissue Eng., Part C*, 2009, **15**(1), 77–85.

152 E. Schnell, et al., Guidance of glial cell migration and axonal growth on electrospun nanofibers of poly-ε-caprolactone and a collagen/poly-ε-caprolactone blend, *Biomaterials*, 2007, **28**, 3012–3025.

153 H. Yoshimoto, et al., A biodegradable nanofiber scaffold by electrospinning and its potential for bone tissue engineering, *Biomaterials*, 2003, **24**, 2077–2082.

154 W.-J. Li, et al., Biological response of chondrocytes cultured in three dimensional nanofibrous poly(ε-caprolactone) scaffolds, *J. Biomed. Mater. Res.*, 2003, **67**(4), 1105–1114.

155 M. Shin, H. Yoshimoto and J. P. Vacanti, In vivo bone tissue engineering using mesenchymal stem cells on a novel electrospun nanofibrous scaffold, *Tissue Eng.*, 2004, **10**(1/2), 33–41.

156 M. Shin, et al., Contractile cardiac grafts using a novel nanofibrous mesh, *Biomaterials*, 2004, **25**, 3717–3723.

157 O. Ishii, et al., In vitro tissue engineering of a cardiac graft using a degradable scaffold with an extracellular matrix-like topography, *J. Thorac. Cardiovasc. Surg.*, 2005, **130**(5), 1358–1363.

158 W.-J. Li, et al., Multilineage differentiation of human mesenchymal stem cells in a three-dimensional nanofibrous scaffold, *Biomaterials*, 2005, **26**, 5158–5166.

159 Y. M. Kolambkar, Electrospun nanofiber meshes for the repair of large bone defects, PhD thesis proposal, Department of Biomedical Engineering, Georgia Institute of Technology, 2007.

160 B. Nottelet, et al., Factorial design optimization and in vivo feasibility of poly(ε-caprolactone)-micro- and nanofiber-based small diameter vascular grafts, *J. Biomed. Mater. Res., Part A*, 2009, **89**(4), 865–875.

161 D. R. Nisbet, et al., Characterization of neural stem cells on electrospun poly(ε-caprolactone) submicron scaffolds: evaluating their potential in neural tissue engineering, *J. Biomater. Sci., Polym. Ed.*, 2008, **19**(5), 623–634.

162 W.-J. Li, et al., Evaluation of articular cartilage repair using biodegradable nanofibrous scaffolds in a swine model: a pilot study, *J. Tissue Eng. Regener. Med.*, 2009, **3**, 1–10.

163 E. Piskin, et al., In vivo performance of simvastatin-loaded electrospun spiral-wound polycaprolactone scaffolds in reconstruction of cranial bone defects in the rat model, *J. Biomed. Mater. Res., Part A*, 2009, **90**(4), 1137–1151.

164 M. Chen, H. Michaud and S. Bhowmick, Controlled vacuum seeding as a means of generating uniform cellular distribution in electrospun polycaprolactone (PCL) scaffolds, *J. Biomech. Eng.*, 2009, **131**(7), 074521.

165 D. R. Nisbet, et al., Neurite infiltration and cellular response to electrospun polycaprolactone scaffolds implanted into the brain, *Biomaterials*, 2009, **30**(27), 4573–4580.

166 J. K. Wise, et al., Chondrogenic differentiation of human mesenchymal stem cells on oriented nanofibrous scaffolds: engineering the superficial zone of articular cartilage, *Tissue Eng. A*, 2009, **15**(4), 913–921.

167 T. T. Ruckh, et al., Osteogenic differentiation of bone marrow stromal cells on poly(ε-caprolactone) nanofiber scaffolds, *Acta Biomater.*, 2010, **6**(8), 2949–2959.

168 H. Wu, et al., Electrospinning of small diameter 3-D nanofibrous tubular scaffolds with controllable nanofiber orientations for vascular grafts, *J. Mater. Sci.: Mater. Med.*, 2010, **21**(12), 3207–3215.

169 Y. B. Zhu, et al., Macro-alignment of electrospun fibers for vascular tissue engineering, *J. Biomed. Mater. Res., Part B*, 2010, **92**(2), 508–516.

170 H. Q. Cao, et al., The topographical effect of electrospun nanofibrous scaffolds on the in vivo and in vitro foreign body reaction, *J. Biomed. Mater. Res., Part A*, 2010, **93**(3), 1151–1159.

171 B. S. Jha, et al., Two pole air gap electrospinning: fabrication of highly aligned, three-dimensional scaffolds for nerve reconstruction, *Acta Biomater.*, 2011, **7**(1), 203–215.

172 L. Ye, et al., Heparin-conjugated PCL scaffolds fabricated by electrospinning and loaded with fibroblast growth factor 2, *J. Biomater. Sci., Polym. Ed.*, 2011, **22**(1–3), 389–406.

173 J. Venugopal, T. Y. L. L. Ma and S. Ramakrishna, In vitro study of smooth muscle cells on polycaprolactone and collagen nanofibrous matrices, *Cell Biol. Int.*, 2005, **29**, 861–867.

174 J. Venugopal, Y. Zhang and S. Ramakrishna, Fabrication of modified and functionalized polycaprolactone nanofiber scaffolds for vascular tissue engineering, *Nanotechnology*, 2005, **16**, 2138–2142.

175 J. R. Venugopal, Y. Zhang and S. Ramakrishna, In vitro culture of human dermal fibroblasts on electrospun polycaprolactone collagen nanofibrous membrane, *Artif. Organs*, 2006, **30**(6), 440–446.

176 S. J. Lee, et al., Development of a composite vascular scaffolding system that withstands physiological vascular conditions, *Biomaterials*, 2008, **29**, 2891–2898.

177 S. Srouji, et al., 3-D Nanofibrous electrospun multilayered construct is an alternative ECM mimicking scaffold, *J. Mater. Sci.: Mater. Med.*, 2008, **19**, 1249–1255.

178 X. Yang, J. D. Shah and H. Wang, Nanofiber enabled layer-by-layer approach toward three-dimensional tissue formation, *Tissue Eng. A*, 2009, **15**(4), 945–956.

179 B. W. Tillman, et al., The in vivo stability of electrospun polycaprolactone–collagen scaffolds in vascular reconstruction, *Biomaterials*, 2009, **30**(4), 583–588.

180 Y. M. Ju, et al., Bilayered scaffold for engineering cellularized blood vessels, *Biomaterials*, 2010, **31**(15), 4313–4321.

181 C. S. Szot, et al., Investigation of cancer cell behavior on nanofibrous scaffolds, *Mater. Sci. Eng., C*, 2011, **31**(1), 37–42.

182 Y. C. Lim, et al., Micropatterning and characterization of electrospun poly(ε-caprolactone)/gelatin nanofiber tissue scaffolds by femtosecond laser ablation for tissue engineering applications, *Biotechnol. Bioeng.*, 2011, **108**(1), 116–126.

183 R. S. Tigli, et al., Cellular behavior on epidermal growth factor (EGF)-immobilized PCL/gelatin nanofibrous scaffolds, *J. Biomater. Sci., Polym. Ed.*, 2011, **22**(1–3), 207–223.

184 P. Wutticharoenmongkol, P. Pavasant and P. Supaphol, Osteoblastic phenotype expression of MC3T3-E1 cultured on electrospun polycaprolactone fiber mats filled with hydroxyapatite nanoparticles, *Biomacromolecules*, 2007, **8**, 2602–2610.

185 C. Erisken, D. M. Kalyon and H. Wang, Functionally graded electrospun polycaprolactone and β-tricalcium phosphate nanocomposites for tissue engineering applications, *Biomaterials*, 2008, **29**, 4065–4073.

186 X. C. Yang, et al., The performance of dental PCL/gelatin/nHA scaffolds pulp stem cells on nanofibrous, *J. Biomed. Mater. Res., Part A*, 2010, **93**(1), 247–257.

This journal is © The Royal Society of Chemistry 2011

J. Mater. Chem., 2011, **21**, 9419–9453 | 9453